https://doi.org/10.5194/essd-2026-420
Preprint. Discussion started: 21 September 2026


# Methane Inversion inter-Comparison (MICA): A Multi-model Estimation of Regional and National Emissions in Asia

Fenjuan Wang[1*], Shamil Maksyutov[1], Rajesh Janardanan[1], Dmitry A. Belikov[2], Prabir K. Patra[3], Ruosi Liang[4,5], Yuzhong Zhang[4], Ge Ren[6,7], Hong Lin[6,7], Nicole Montenegro[8], Antoine Berchet[8], Marielle Saunois[8], Adrien Martinez[8], Sara Hyvärinen[9], Aki Tsuruta[9], Samuel Takele Kenea[10], Miao Liang[11], Xin Lan[12,13], Yukio Terao[1], Md. Kawser Ahmed[14], Manish Naja[15], Akihiko Ito[16], Isamu Morino[1],Yukio Yoshida[1], Yu Someya[1],Tazu Saeki[1], Tsuneo Matsunaga[1]

[1]Satellite Observation Center, National Institute for Environmental Studies, Tsukuba, 305-8506, Japan
[2]Chiba University, Chiba, 263-8522, Japan
[3]Research Institute for Global Change, JAMSTEC, Yokohama 236-0001, Japan
[4]School of Engineering, Westlake University, Hangzhou, China
[5]Now at Southern University of Science and Technology, Shenzheng, China
[6]National Institute of Metrology of China, Beijing, China
[7]Zhengzhou Institute of Metrology, Zhengzhou, China
[8]Laboratoire des Sciences du Climat et de l'Environnement, LSCE-IPSL (CEA-CNRS-UVSQ), Université Paris-Saclay, 91191 Gif-sur-Yvette, France
[9]Finnish Meteorological Institute, Helsinki, Finland
[10]Global Watch Atmosphere and Research Division, National Institute of Meteorological Sciences, 33, Seohobuk-ro, Seogwipo-si 63568, Jeju-do, Korea
[11]Meteorological Observation Center, China Meteorological Administration, Beijing 100081, People's Republic of China
[12]Cooperative Institute for Research in Environmental Sciences, University of Colorado Boulder, Boulder, CO 80309, USA
[13]Global Monitoring Laboratory, National Oceanic and Atmospheric Administration (NOAA), Boulder, CO 80305, USA
[14]Department of Oceanography, Faculty of Earth and Environmental Sciences, University of Dhaka, Dhaka-1000, Bangladesh
[15]Atmospheric Science Division, Aryabhatta Research Institute of Observational Sciences, Nainital, India
[16]The University of Tokyo, Tokyo, Japan

[*]*Correspondence to:* Fenjuan Wang (wang.fenjuan@nies.go.jp)

**Abstract** Accurate quantification of methane ($CH_4$) emissions from countries/regions is essential for effective emission reduction policy, but large uncertainties persist due to sparse observations and divergent bottom-up inventories. This study establishes a top-down Asian regional methane emission dataset based on the Methane Inversion inter-Comparison for Asia (MICA), using an ensemble of seven inversion systems (five global, two regional) assimilating surface in-situ measurements and GOSAT satellite retrievals for 2010–2021 under a common protocol. Validation against independent surface, aircraft, and balloon data demonstrates substantial improvements in model performance after inversion, with significant reductions in model-observation Root Mean Square Error (RMSE). Posterior estimates indicate an overall reduction of prior emissions by ~15% for the study area, with the largest decline in East Asia (~25.8%). Though a systematic downward adjustment by the inversion ensemble is observed for most top emitting-countries, the median differences between posterior and prior emissions vary across countries, from -0.9% (Mongolia) to -16.2% (China). Sectoral results suggest increasing emissions from waste management across developing Asian countries and a fourfold increase in Indonesian coal-mine emissions. Comparisons with National Greenhouse Gas Inventories (NGHGIs) reveal systematic underreporting by several nations—notably India, Pakistan, and Bangladesh. We find that inter-model spread is driven largely by horizontal resolution (Coefficient of Variation 10–20%), and that joint assimilation of satellite and surface observations is an effective option for constraining emissions in regions with sparse monitoring or

https://doi.org/10.5194/essd-2026-420
Preprint. Discussion started: 21 September 2026




complex land–sea geometries. This dataset provides a foundation for regional and national methane budget assessment in Asia and inverse model development, with robust consistency across multiple inversion systems and independent observations. The dataset generated in this study is openly available via Zenodo (https://doi.org/10.5281/zenodo.22699291, Wang et al., 2026).

## 1 Introduction

Global atmospheric methane ($CH_4$) concentration has been rising at a record speed since 2014 (Nisbet et al., 2016, 2019), with the fastest growth occurring over the last four years from 2020 through 2023 (Lan et al., 2022). This recent acceleration follows a period of stabilization from the late 1990s to 2006 (Dlugokencky et al., 1998, 2003; Etheridge et al., 1998) and a renewed increase that began in 2007 (Dlugokencky et al., 2009, 2011; Nisbet et al., 2014). Since the Industrial Revolution, methane levels have nearly tripled, making it the second most impactful anthropogenic greenhouse gas after carbon dioxide ($CO_2$) (IPCC, 2023). The increase in atmospheric methane concentrations poses a significant challenge to achieving global climate goals, particularly those outlined in the Paris Agreement (Fletcher and Schaefer, 2019; Tanimoto et al., 2025). Methane is a potent greenhouse gas, which affects the Earth's energy budget through its direct radiative effect and indirect influence on ozone, water vapor, and $CO_2$, makes its reduction critical for near-term climate stabilization (Jackson et al., 2024; O'Connor et al., 2022; Watts et al., 2026).

Methane emissions originate from a variety of natural sources, including wetlands, inland freshwaters, geological sources, and biomass burning, as well as anthropogenic activities (Saunois et al., 2020). A substantial portion of this global increase is driven by anthropogenic emissions from agriculture (ruminant livestock and rice farming), fossil fuel exploitation, and waste management (Jackson et al., 2024; Schaefer, 2019; Schaefer et al., 2016). Asia is a prominent contributor to these emissions (Niwa et al., 2024; Stavert et al., 2022; Yin et al., 2021). Recent studies have evaluated Asia's methane budgets using various methods. Bottom-up estimates, which rely on inventories, indicted that East Asia was a net source of 67.3 ± 14 Tg $CH_4$ $yr^{-1}$ between 2000 and 2012, with anthropogenic emissions accounting for 88.8% (Ito et al., 2019). A comprehensive assessment for 1970-2021 further highlighted that anthropogenic sources were responsible for 84% of total emissions in the 2010s, with notable regional variations (Ito et al., 2023). To evaluate and improve these bottom-up inventories, top-down approaches that use atmospheric measurements are essential. Data from ground-based observations and satellite remote sensing, such as Greenhouse gases Observing SATellite (GOSAT) (Kuze et al., 2009) and TROPOspheric Monitoring Instrument (TROPOMI) (Hu et al., 2016), are used to constrain inverse models to estimate emissions in part of Asia region (Liang et al., 2024; Nomura et al., 2021; Patra et al., 2016; Qin et al., 2025; Thompson et al., 2015; Wang et al., 2024). Wang et al. (2019) estimated average top-down $CH_4$ budgets for the period 2009-2018 as 63.40, 45.20, and 64.35 Tg $CH_4$ $yr^{-1}$ for East, Southeast, and South Asia, respectively. While these top-down estimates provide critical insights, they frequently show divergences at finer scales, indicating persistent uncertainties (Janardanan et al., 2024; Kirschke et al., 2013; Saunois et al., 2016). Addressing these uncertainties is key to effective climate action, especially as nations like China are taking steps to control methane emissions (You, 2024). Significant challenges persist, notably the uncertainties inherent in computational models and the discrepancies observed between disparate data sources (Houweling et al., 2017; Jacob et al., 2022). Multi-group intercomparisons, which compare results from multiple models and data sets,

https://doi.org/10.5194/essd-2026-420
Preprint. Discussion started: 21 September 2026




have proven effective for yielding robust large-scale flux estimates (Chiao et al., 2010; Houweling et al., 2015). Such studies have been conducted on the global scale (Jackson et al., 2024; Kirschke et al., 2013; Saunois et al., 2016, 2020, 2025) and within specific regions, such as Europe (Ioannidis et al., 2026; Monteil et al., 2020) and North American (Poulter et al., 2025). However, a comprehensive multi-group intercomparison study for the broader Asian region has yet to be reported, although contributions have been made at the subregional level (Kondo et al., 2025).

Hence this study presents the first multi-model intercomparison specifically for the Asia region. Our research, conducted under the protocol for Methane Inversion inter-Comparison – evaluation of methane emissions at regional and national scale for the Asian region (MICA), addresses the following key objectives:

1. Assess the constraints of atmospheric measurements on country-level methane fluxes, with a particular focus on long-term emission trends.
2. Evaluate methane emissions in key Asian regions (East Asia, South Asia, Southeast Asia, and major Asian emitting-countries).
3. Investigate sectoral anthropogenic and natural emissions, their associated uncertainties, and the added value of satellite-based $XCH_4$ observations in constraining methane fluxes.
4. Build an open-access dataset of top-down emission estimates, useful for inverse model development, gridded inventory benchmarking, and comparison with national inventory reports.

Due to rapid changes in Asian methane emissions and expanding observation networks, international intercomparisons intend to be conducted every five years depending on participant availability and interest.

## 2 Data and Methods

### 2.1 The MICA Intercomparison Protocol

The MICA protocol was established to provide a standardized framework for evaluating and intercomparing $CH_4$ flux inversions. Participants are required to use a common set of atmospheric observations and priori $CH_4$ emissions, as detailed in Sections 2.2 and 2.3, respectively. Participants are required to submit prior and posterior fluxes and their corresponding uncertainties for gridded fluxes, national totals, and simulated concentrations. The regional inversion domain spans from 60°E to 152°E and 15°S to 54°N. Although spatial resolution remains at the discretion of the participants, submission of national and regional emission totals is mandatory adhering to the standardized masks defined in Section 2.4. Additionally, a dedicated validation dataset has been established to evaluate model performance. Participants conducting global or regional flux inversion simulations are encouraged to cover the 12-year period from January 1, 2010, to December 31, 2021. The experimental protocal utilizes the following $CH_4$ datasets:

Experiment 1 (Mandatory): Baseline simulation utilizing surface $CH_4$ observations (SURF).

Experiment 2 (Optional): Simulation utilizing GOSAT $XCH_4$ retrievals (GOS).

https://doi.org/10.5194/essd-2026-420
Preprint. Discussion started: 21 September 2026


Further details regarding atmospheric measurements, prior emissions, participating models, inversion techniques, and simulation outputs are provided in the following subsections.

### 2.2 Atmospheric Observations and region definition

The observation data used in this study were collected from various sources to provide a comprehensive view of $CH_4$ observations in Asia. The dataset includes the $XCH_4$ data of GOSAT (NIES Level 2 product, v.03.05) (Someya et al., 2023; Yoshida et al., 2011), as well as the recent versions of the Obspack$CH_4$ ground-based data sets (detailed in Table S1 in the supplementary): obspack_ch4_1_GLOBALVIEWplus_v5.1_2023-03-08 and obspack_ch4_1_NRT_v5.1_2023-02-21 (Schuldt et al., 2023). To supplement these, additional ground-based observations were incorporated from a network of stations across Asia, including four sites from NIES (National Institute for Environment Studies, Japan) seven sites from CMA (China Meteorological Administration), one from KMA( Korea Meteorological Administration), and four from the WDCGG (World Data Centre for Greenhouse Gases) with a detailed list provided in Table S2. Figure.1 shows the locations of the measurement sites in the domain including sites used in inversion systems and independent validation. The distribution of GOSAT observations is shown in Figure. S1 in the supplementary. Given that many of the CMA stations are located in areas with intense local emissions, their measurements were filtered to distinguish between regional-scale data and locally contaminated readings. Only data classified as "regional events," which are representative of concentrations over a wide area, were used in our analysis, ensuring the robustness of our conclusions regarding large-scale $CH_4$ levels. This filtering methodology is described in more details by (Zhang et al., 2022a; Zhang et al., 2022b). The study area encompresses three regions: East Asia (China, Mongolia, Japan, South Korea, and North Korea), South Asia (India, Pakistan, Nepal, Maldives, Bhutan, Bangladesh, and Afghanistan), and Southeast Asia (Indonesia, Malaysia, Cambodia, Myanmar, Laos, Baker Island, the Philippines, Singapore, Thailand, Timor-Leste, and Vietnam).

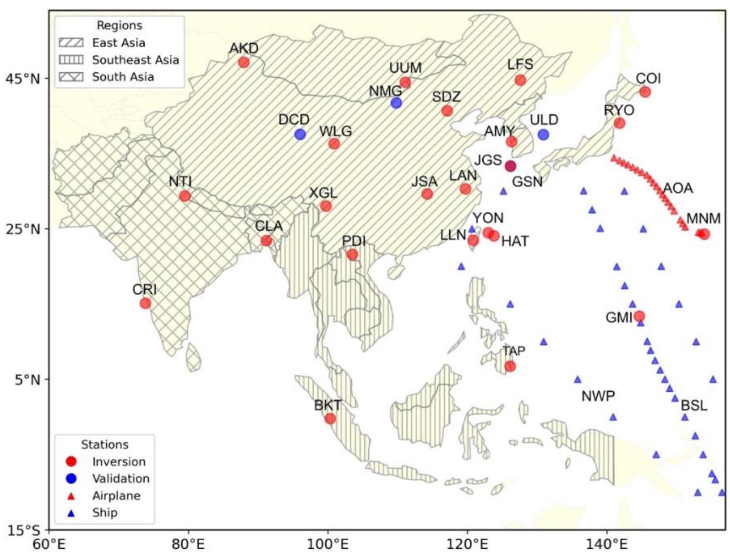


**Figure 1:** Locations of observation stations used in this study. Shaded hatching patterns indicate the regions East Asia, Southeast Asia, and South Asia. Airplane measurements are denoted by AOA, ship-based measurements by BSL and NWP,

https://doi.org/10.5194/essd-2026-420
Preprint. Discussion started: 21 September 2026


and balloon measurement sites by DCD and NMG. The country map was generated with ne_110m_admin_0_countries v5.1.1, (download from https://www.naturalearthdata.com/).

### 2.3 Prior Emission Inventories

We specify the prior $CH_4$ fluxes prescribed for this experiment. These data are provided at a monthly temporal resolution and on a 0.1° x 0.1° global spatial grid, along with their original source resolutions to accommodate the specific requirements of different modeling systems. The prior fluxes combine a synthesis of multiple inventories, the components of which are detailed in Table 1. Anthropogenic emissions are based on the EDGAR v7 (Emissions Database for Global Atmospheric Research) inventory (Crippa et al., 2021), with monthly variations derived from EDGAR v6 data. To prevent double-counting, agricultural waste burning is excluded from the total flux, as it is already accounted for in the biomass burning data. Natural sources include VISIT (Vegetation Integrative SImulator for Trace gases) model simulations for global wetland emissions and soil sinks (Ito and Inatomi, 2012). Biomass burning emissions are from the Global Fire Assimilation System (GFAS) (Kaiser et al., 2011). Finally, climatological estimates for termites, oceans, geological sources, and freshwater are based on datasets from the Global Carbon Project (GCP) (Saunois et al., 2025). Spatial distributions of prior fluxes are presented in Figure S2.

**Table 1:** Prior $CH_4$ fluxes used in this study.

| Category | Data source | Spatiotemporal resolution | | Time period |
|---|---|---|---|---|
| Coal, Agriculture, Waste, Biofuels, Oil, Gas & Industry | EDGAR v7.0<br>EDGAR v6.0 | 0.1° × 0.1° | Monthly | 2009-2021 |
| Fire | GFAS | 0.1° × 0.1° | Daily | 2009-2021 |
| Wetland, Soi sink | VISITv20230209b | 0.5° × 0.5° | Monthly | 2009-2021 |
| Termites | (Saunois et al., 2025) | 0.1° × 0.1° | Monthly | Climatology |
| Ocean | (Weber et al., 2019) | 0.1° × 0.1° | Monthly | Climatology |
| Geological | (Etiope et al., 2019) | 0.1° × 0.1° | Monthly | Climatology |
| Freshwater | (Saunois et al., 2025) | 0.1° × 0.1° | Monthly | Climatology |

### 2.4 Atmospheric Models and Inverse Systems

This study utilizes a multi-model ensemble of six state-of-the-art atmospheric transport models and their respective inverse modeling systems, including CTE-CH4, GEOS-Chem, LMDZ, MIROC4-ACTM, NTFVAR, and NTLB. These systems employ diverse transport models, meteorological data, and inversion algorithms ranging from 4D-variational (4D-Var) to Ensemble Kalman Filters (EnKF) and Bayesian approaches to optimize regional and global emissions.

The CTE-CH4 (CarbonTracker Europe-CH4) system utilizes the TM5 transport model (Krol et al., 2005) driven by within ERA5 meteorology, within an ensemble Kalman smoother framework (Peters et al., 2005; Van Der

https://doi.org/10.5194/essd-2026-420
Preprint. Discussion started: 21 September 2026


Open Access Earth System Science Data Discussions

Laan-Luijkx et al., 2017). It optimizes anthropogenic and wetland+soil fluxes separately globally. The system employs 150 ensemble members and a 5-week lag window to account for long-range transport (Bruhwiler et al., 2014; Tsuruta et al., 2017).

The nested regional version of the GEOS-Chem model (v12.9.3) is applied for the Asian domain. The simulation is driven by MERRA-2 meteorological data (Gelaro et al., 2017) at 0.5° × 0.625° horizontal resolution with 47 vertical layers. Monthly $CH_4$ fluxes from 600 spatial clusters, generated using a Gaussian mixture model algorithm (Turner and Jacob, 2015), are optimized with the analytical solution to the Bayesian inversion, assimilating high-density satellite and in situ data streams (East et al., 2025; Liang et al., 2023, 2024; Zhang et al., 2022b).

The LMDZ-SACS system isd into the Community Inversion Framework (CIF), enabling unified variational or ensemble-based optimizations (Berchet et al., 2021). It couples the LMDz general circulation model (Hourdin et al., 2006) with the Simplified Atmospheric Chemistry System (SACS) to simulate oxidation processes (Pison et al., 2009). CIF enables efficient parallelization and the assimilation of multi-species data, including isotopes (Thanwerdas et al., 2024). In this study, we employ a 4D-Var approach using the M1QN3 optimization algorithm. Prior error correlations are prescribed with spatial length scales ranging from 500 to 1,500 km and temporal scales from 1 to 6 months with sector-specific values detailed in Montenegro et al. (2025).

The MIROC4-ACTM model is an atmospheric chemistry-transport model within a time-dependent Bayesian approach to estimate monthly emissions across 54 land regions (Patra et al., 2016). The model is nudged to JRA-55 reanalysis to ensure realistic transport (Patra et al., 2018). It includes a posterior loss correction method to balance the global budget and has been extensively validated against GOSAT and aircraft observations (Belikov et al., 2024; Chandra et al., 2021).

The NTFVAR (NIES-TM-FLEXPART-variational) system is a high-resolution 4D-variational inversion framework that couples the Eulerian model NIES-TM for global background transport with the Lagrangian model FLEXPART for near-field sensitivity (Belikov et al., 2016; Maksyutov et al., 2021). The system uses ERA5 and JRA-55 (Kobayashi et al., 2015) meteorological data, with a 50 km spatial correlation length to ensure smoothness. The inversion optimizes six source categories via bi-weekly scaling factors. Its robust performance has been validated through sensitivity tests and extensive budget studies (Janardanan et al., 2024; Wang et al., 2019, 2025a).

The NTLB ('NIM-TM-LTM-BAY) regional system couples the WRF (v4.3) meteorological model (Grell et al., 2005) with the STILT Lagrangian particle dispersion model (Lin et al., 2003). WRF is initialized with NCEP FNL data and provides 27 km resolution footprints over the study domain. The system uses a Bayesian framework to estimate monthly fluxes, with a 500 km prior correlation length (Ren et al., 2024; Yadav and Michalak, 2013).

https://doi.org/10.5194/essd-2026-420
Preprint. Discussion started: 21 September 2026




Table 2 and Table 3 further summarize the key atmospheric model and inverse configuration parameters for the six models. These parameters define how each system handles uncertainties, spatial/temporal relationships, and the observational constraints that drive the posterior flux estimates.

**Table 2:** Summary of atmospheric inverse modeling systems.

| Model System | Institute | Atmospheric model | Horizontal/vertical resolution | Modele type | Inverse Method | Meteorology |
|---|---|---|---|---|---|---|
| CTE-CH4 | FMI | TM5 | Region-wise (global) 1° × 1° (regional)/ 25 levels | Eulerian | EnKF | ERA5 |
| GEOS-Chem | WLU | GEOS-Chem v12.9.3 | 0.5° × 0.625° (regional)/ 47 levels | Eulerian | Bayesian | MERRA-2 |
| LMDZ | LSCE | LMDz v6 | 2.5° × 1.27° (global) / 79 levels | Eulerian | 4D-Var (CIF) | ERA5 |
| MIROC4-ACTM | JAMSTEC | MIROC4-ACTM | 2.8° × 2.8° (global) / 67 levels | Eulerian | Bayesian | JRA-55 |
| NTFVAR | NIES | NIES-TM / FLEXPART | 3.75° × 3.75° (global) (NIES-TM), 0.1° × 0.1° (FLEXPART)/ 42 levels | Coupled Eulerian-Lagrangian | 4D-Var | ERA5/ JRA-55 |
| NTLB | NIM | WRF-STILT | 0.27° × 0.27° (regional)/ 35 levels | Coupled Eulerian-Lagrangian | Bayesian | NCEP FNL |

**Table 3:** Inverse configuration and uncertainty parameters.

| Model System | Window/ Lag | Prior Flux Uncertainty | Correlation Length (Space/ Time) | Model-Data Mismatch | Optimized fluxes |
|---|---|---|---|---|---|
| CTE-CH4 | 7-day/ 5 weeks | 80% | 300 km/ No time corr. | 4.5–75 ppb | sectoral (anthropogenic and wetland + soil sink) |
| GEOS-Chem | 1 month | 50% | No | ~18 ppb for satellite and ~30 ppb for surface data (location dependent) | total |
| LMDZ | 12-month | 100% for total flux | 500 km/ 1 month | 3–15 ppb (remote), >30 ppb (urban) | sectoral |
| MIROC4-ACTM | 1 month | 30% for total flux | Regional (54 regions) | 10–50 ppb (location dependent) | total |

https://doi.org/10.5194/essd-2026-420
Preprint. Discussion started: 21 September 2026


| | | | | | |
|---|---|---|---|---|---|
| NTFVAR | 2 weeks | 30% of anthropogenic and 50% of wetland | 50 km/ 2 weeks | 15–30 ppb (site-specific) | sectoral (anthropogenic and wetland) |
| NTLB | 1 month | 30% | 500 km/ 1 month | 28 ppb | total |

### 2.5 Dataset products and Data Processing

An overview of the dataset products and their simulation periods is provided in Table 4, complemented by a detailed description provided in the Readme file. The dataset repository provides a comprehensive collection of standardized outputs from each participating inverse model. These include high-resolution monthly spatial fluxes (grid_[exp]_[model].nc), easily accessible integrated monthly national or regional/sectoral summaries (emis_[exp]_[model].csv or emis_[exp]_[model].nc), ensemble mole fraction concentrations (conc_[exp]_[model].csv), and independent model validation records (val_[exp]_[model].csv). All participating models performed a baseline simulation (SURF), constrained by surface CH4 observations. In addition, four models submitted results for a supplementary simulation (GOS), which used GOSAT XCH4 retrievals. Sectoral information is not uniformly reported or included across all participating inverse models, as detailed below. Two submissions were provided by NIES: NTFVAR using the proposed prior emissions, and NTFVAR2 using the GCP prior for comparison. The MIROC4-ACTM simulations used surface observations from the World Data Centre for Greenhouse Gases (WDCGG), following the configuration described in Belikov et al. (2024). The GEOS-Chem GOS simulations used GOSAT (UoL, v9.0) data (Parker and Boesch, 2020).

**Table 4:** Overview of dataset products generated by the participating inverse models.

| Model | Experiment exp1(SURF) exp2(GOS) | Gridded Fluxes grid*.nc | Country Totals emis*.csv emis*.nc | $CH_4$ mixing ratios conc*.csv | Validation val*.csv | Sectorer |
|---|---|---|---|---|---|---|
| CTE-CH4 | SURF, GOS | ✓ | ✓ | ✓ | ✓ | ✓ |
| GEOS-Chem | SURF, GOS | ✓ | ✓ | ✓ | ✓ | ✓ |
| LMDZ | SURF, GOS | ✓ | ✓ | ✓ | ✓ | ✓ |
| MIROC4-ACTM | SURF | ✓ | ✓ | ✓ | ✓ | |
| NTFVAR | SURF, GOS | ✓ | ✓ | ✓ | ✓ | ✓ |
| NTFVAR2 | SURF | ✓ | ✓ | ✓ | ✓ | ✓ |
| NTLB | SURF | ✓ | ✓ | ✓ | ✓ | |

https://doi.org/10.5194/essd-2026-420
Preprint. Discussion started: 21 September 2026




National total emissions were aggregated from grid-based flux data using a standardized country mask to enable cross-model intercomparison. In this study, we employed the countrymask_eez, which represents the union of global national boundaries and Exclusive Economic Zones (EEZ) (Marine Regions, 2018). The primary reason for selecting the countrymask_eez is the presence of significant offshore $CH_4$ emissions within the study domain, particularly from natural gas production. Several countries in the Asian region, including Indonesia, the Philippines, Vietnam, and Malaysia, have substantial offshore activities that contribute noticeable $CH_4$ emissions. We compared national total emissions aggregated from the EDGAR v7 gridded flux data using both the land-only country mask and the countrymask_eez. As a result, the aggregated totals using the countrymask_eez are in much closer agreement with the officially reported national totals in the EDGAR v7 dataset (detailed in Table S3). Notably, the differences are particularly pronounced for South and Southeast Asian countries with significant offshore production, further supporting the adoption of the countrymask_eez in this intercomparison.

# 3 Results: Methane Emission Estimates

## 3.1 Regional Methane Estimates

In this section, we evaluate the posterior emission adjustments by comparing the spatial patterns and temporal correlations of the multi-model ensemble against the prior inventories.

Figure 2 illustrates the spatial distribution of a representative prior flux and posterior corrections (posterior minus prior) driven from the inverse models constrained by surface-only data. While spatial patterns of these corrections vary among the models, some consistent spatial patterns are discernible. Models including CTE-CH4, GEOS-Chem, LMDZ, NTFVAR, and NTLB show a significant reduction in fluxes over East Asia, particularly in southeastern China. Conversely, CTE-CH4 depicts some flux increases in northern China. NTFVAR2 shows upward corrections across northern China, including areas with dense coal emission sources in the North China Plain, which may be attributed to the underestimation of gas and oil emissions in the Greenhouse Gas and Air Pollution Interactions and Synergies (GAINS) prior inventory, which differed from the protocol (Janardanan et al., 2024). In South Asia, results exhibit higher inter-model variability, due to the lack of observational constraint. While most models indicate downward corrections, GEOS-Chem and MIROC4-ACTM show upward adjustments, particularly over wetland areas in Bangladesh and Myanmar. A large variability is also observed in the Southeast Asian regions. Some models (LMDZ, NTFVAR, NTFVAR2, NTLB) show reductions, while others (CTE-CH4, MIROC4-ACTM) indicate upward corrections, and GEOS-Chem shows very few adjustments. The variation in Southeast Asia is also clearly seen from the GOSAT-only constraint corrections shown in Figure S3. This significant discrepancy underscores the uncertainty in the posterior fluxes and highlights the regional differences in model constraints and the inverse corrections.

https://doi.org/10.5194/essd-2026-420
Preprint. Discussion started: 21 September 2026


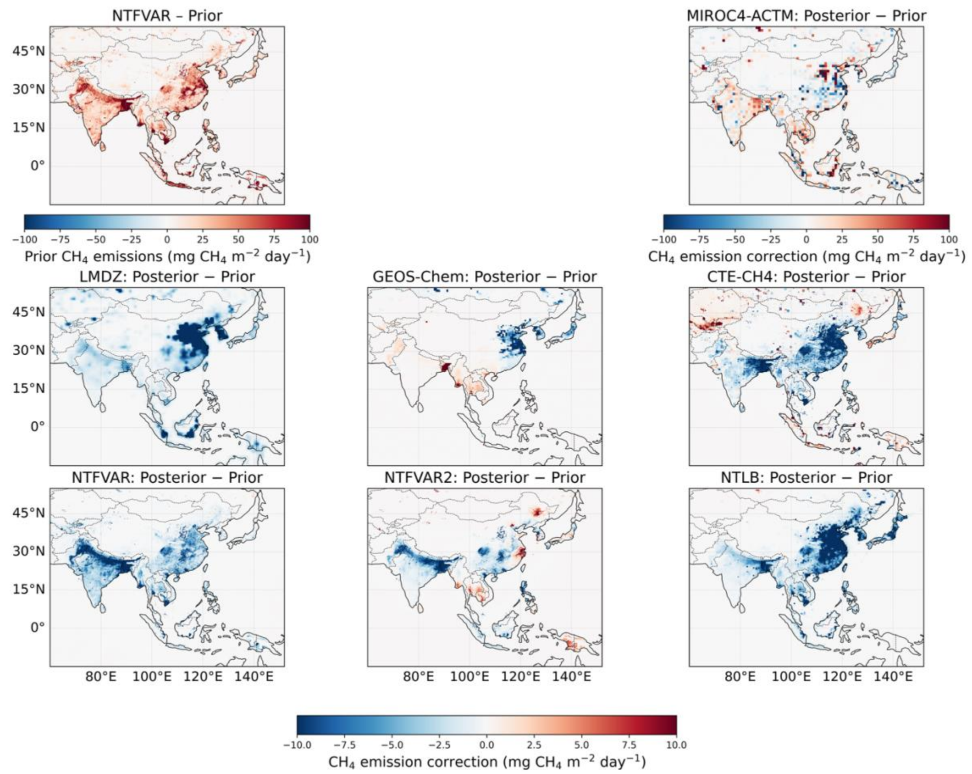


**Figure 2:** Spatial distribution of prior fluxes and model-specific posterior corrections averaged over simulation period. The upper-left panel shows the reference averaged prior emissions baseline. Other panels show the average flux corrections (posterior minus prior) calculated for each respective simulation based on surface-only $CH_4$ observations (SURF).

Figure 3 presents the prior and posterior $CH_4$ emissions for each subregion and the entire domain over the period 2010–2021 by surface-only data. Posterior emissions show consistent downwards adjustments across all regions relative to the prior emissions, reflecting the influence of observational constraints. Over the study period, the average total posterior emissions decreased by approximately 15% compared to prior emissions. Regionally, the most significant reduction was observed in East Asia (25.8%), followed by South Asia (10.4%) and Southeast Asia (6.4%). Regional variability in the prior estimates is primarily driven by the disparity in spatial resolution across the ensemble and the specific emission inventories adopted by NTFVAR2, as detailed in the comparative analysis in Section 4.1. Notably, the spread among posterior emissions is reduced for East Asia, and Southeast Asia, indicating improved inter-model consistency following inverse optimization. In contrast, South Asia exhibits a wider spread in posterior estimates, likely due to sparse observational coverage, which limits the models' capacity to effectively constrain regional emissions. The Mann–Kendall trend test revealed statistically significant increasing trends ($p < 0.05$) in the prior emissions across the entire domain and all subregions. Posterior emissions also preserved these increasing trends, generally consistent with the prior.

https://doi.org/10.5194/essd-2026-420
Preprint. Discussion started: 21 September 2026



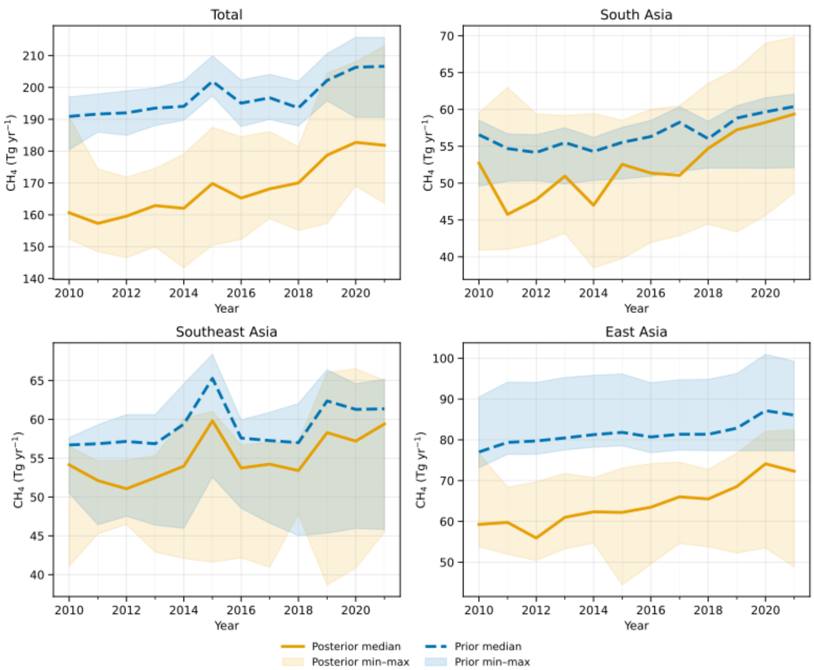


**Figure 3:** Prior and posterior methane emissions for the total and subregions including East Asia, South Asia, and Southeast Asia. The shaded areas represent the minimum–maximum range, and the solid lines indicate the median values.

### 3.2 Comparison of Surface-based and GOSAT-based Inversions

The choice of observational constraints significantly impacts inverse modeling results. This is illustrated by comparing surface-only simulations (SURF) and GOSAT-only simulations (GOS) from models—CTE-CH4, LMDZ, and NTFVAR—each covering the full period from 2010 to 2021. The GEOS-Chem model only provided simulations for 2018–2021, and these results are not presented here to avoid inconsistencies arising from differing simulation periods. Figure 4 reveals that GOS consistently exhibits a larger maximum-minimum range compared to SURF, consistent with previous studies (e.g. Deng et al., 2025) that find column measurements from satellites generally provide a weaker constraint than high-precision surface observations. This larger uncertainty in GOS is likely attributable to the lower sensitivity of GOSAT retrievals to local surface fluxes.

The paired t-test results reveal that the impact of observational constraints (SURF vs. GOS) varies significantly by region. Overall, the simulations differ significantly ($t = 3.22$, $p < 0.01$), with SURF yielding higher total estimates by approximately 4.98 Tg yr$^{-1}$. However, the regional behavior is divergent: in Southeast Asia, SURF estimates are significantly higher than GOS ($t = 8.22$, $p < 0.001$), whereas in East Asia, the trend reverses, with GOS producing significantly higher estimates than SURF ($t=-7.03$, $p < 0.001$). In contrast, South Asia shows no statistically significant difference ($p=0.21$), suggesting the two methods yield comparable results in that region.

https://doi.org/10.5194/essd-2026-420
Preprint. Discussion started: 21 September 2026



These findings highlight that the choice of simulation constraint does not produce a uniform shift, but rather triggers localized adjustments in emission estimates.

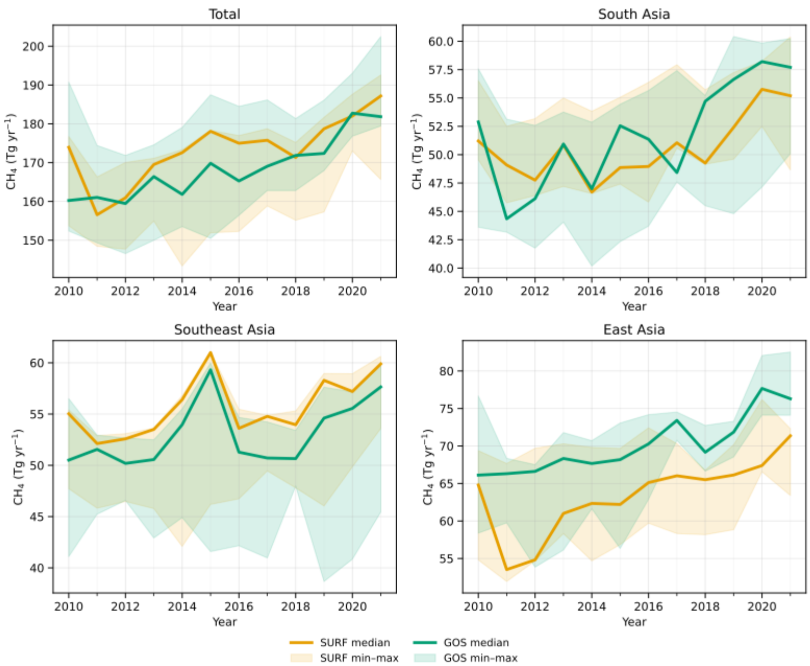


**Figure 4:** Regional annual emissions simulated by inverse models. The shaded areas represent the inter-model range (maximum–minimum) within surface-only simulations (SURF) and GOSAT-only simulations (GOS), while the solid lines denote the median values across models.

### 3.3 National Methane Budgets

Our study domain includes 28 countries, some of which have relatively small areas or low emission levels. To minimize aggregation errors inherent in the inversion process (discussed in Section 4.3), our analysis focuses on 13 "top-emitting" countries where anthropogenic emissions exceeded 1 Tg yr$^{-1}$ during the 2019–2021 period. The inversion results presented here thus emphasize these representative countries to better capture spatial and sectoral emission characteristics across the region. Anthropogenic $CH_4$ emissions constitute the dominant component of the total $CH_4$ budget within the study region, though the magnitude and temporal trends vary considerably by nations. Figure 5 presents the posterior ensemble distributions for these 13 nations, partitioned into anthropogenic and total fluxes, benchmarked against official National Greenhouse Gas Inventories (NGHGIs) and prior ensemble medians. Across all 13 countries, posterior total medians are consistently lower than their corresponding prior medians, indicating a systematic downward adjustment by the inversion ensemble, a trend consistent with the regional flux distributions illustrated in Figure 2 and Figure S3. The relative median differences range from -0.9% (Mongolia) to -16.2% (China). For the first big emitters group (Figure 5(a)), China shows the most pronounced reductions, with the posterior median decreasing from 77.46 to 64.88 Tg yr$^{-1}$. Indonesia and Pakistan exhibit moderate downward shifts of -8.4% and -5.3%, respectively, while India shows only a minor reduction of 1.8%. Most of the other two groups (Figure 5 (b) and (c)), exhibit

https://doi.org/10.5194/essd-2026-420
Preprint. Discussion started: 21 September 2026



moderate downward revisions less than 10%, except South Korea (11.9%). The uniform direciton of these adjustments suggests that, at the ensemble level, prior total $CH_4$ emissions has likely been systematically overestimated for these nations. However, the interquartile ranges (IQRs) of these posterior estimates (box plot) remain substantial for major emitters, reflecting persistent structural differences among inversion systems. When normalized by the median, relative spread is generally 10–20% for major emitters but notably higher for several smaller countries, such as Mongolia (~32%) and Japan (~22%). This persistent spread reflects fundamental structural differences stemming from variations in transport model resolution, physics, chemical loss representations, inversion methods, and the relative weighting of observations. Notably, anthropogenic posterior estimates frequently show smaller inter-model dispersion than total emissions, implying that natural flux components, such as wetlands and freshwater sources, contribute disproportionately to ensemble uncertainty.

The estimated anthropogenic emissions were compared with NGHGIs, as shown in Figure 5 (2019-2021) and Figure 6 (2010-2021). The submission of NGHGIs in this region is limited to only 15 countries that have submitted inventories. Japan and South Korea, as Annex I countries, provide consistent annual reports. The submissions from the developing (non-Annex I) countries are often intermittent, with a high variability ranging from multiple reports to only one or two total submissions. This infrequent and variable reporting schedule contributes to significant regional data gaps, as exemplified by the current unavailability of data for key nations such as the Philippines and Myanmar. Conversely, NGHGIs for Vietnam and Malaysia are substantially higher than our posterior estimates, suggesting potential overestimation in their reported fluxes, or underestimation by models due to lack of observational constraint on fluxes. China's NGHGI exceeds our median estimate, although the most recent 2020 report demonstrates strong alignment with our results. This is consistent with Wang et al. (2025b), who found that China's NGHGI estimates typically fall within the upper bound of the inversion-derived range. Such convergence across different methodologies provides a robust reference point, further corroborated by independent top-down estimates from TROPOMI satellite observations for 2023 (East et al., 2025). Finally, A systematic underestimation is evident in several countries including India, Pakistan, Indonesia, Bangladesh, Thailand, Japan, and Mongolia, where reported emissions are lower than our top-down estimates. These findings align with recent literature (e.g. East et al., 2025) which recommends upward inventory revisions for India, Japan, Bangladesh, and Thailand. This discrepancy, however, may occasionally be obscured by the statistical spread of the models; for instance, some published upward top-down corrections for India remain within the margin of model uncertainty (Janardanan et al., 2020).

https://doi.org/10.5194/essd-2026-420
Preprint. Discussion started: 21 September 2026




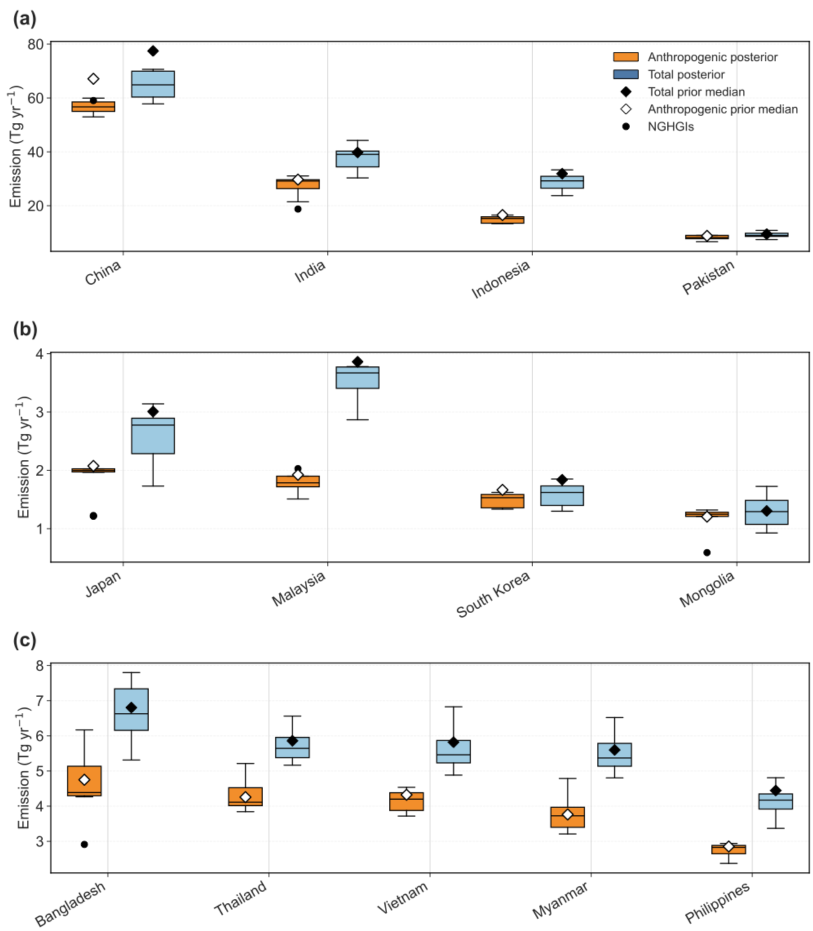


**Figure 5:** National-level boxplots of methane emissions (Tg yr$^{-1}$) over 2019–2021 for anthropogenic (left) and total (right) emissions, based on posterior ensemble results across all inversion models. NGHGI values are shown as black dots. The medians of prior total and prior anthropogenic emissions are shown as diamonds for references. Boxes show the interquartile range (25th–75th percentile) minimum and maximum, with the median indicated by a horizontal line.

### 3.4 Sectoral Emissions and Trends

The sectoral trends in methane emissions from agriculture, coal, oil and gas, waste and wetlands were evaluated for the period 2010-2021 using the Mann-Kendall trend test (Gilbert, 1988), with statistical significance defined at $p<0.05$. Agriculture is the dominant emission source across Asia, with posterior emissions of 64.69 Tg yr$^{-1}$ (62.16–69.94 Tg yr$^{-1}$), since this region accounts for over 90% of global rice production. Driven primarily by rice cultivation and livestock activities, the agricultural sector contributes more than 50% of total anthropogenic emissions in most study countries, with expectations in China (~33%) and Indonesia (~26%) (blue chart in Figure 6). Significant increasing trends were observed in India, Pakistan, Myanmar, and Mongolia. In India, and Pakistan these increases are linked to the continuous expansion of rice-harvested area. Furthermore, rapid livestock growth has intensified emissions. In Pakistan, cattle populations rose from 35 million to 55 million between 2010 and 2021, while Mongolia's cattle population more than doubled from 2.18 million to 5.02 million during the same period. These increases were accompanied by a similar upward trend in sheep and goat populations (Our World in Data, 2024b). In contrast, Japan and Malaysia exhibited statistically significant decreasing trends in agriculture emissions. These declines are largely attributed to the contraction of rice paddy acreage in both countries and a reduction in livestock numbers specifically in Malaysia. For the remaining countries in Figure 6, no statistically significant trends were detected during the period. In China, Zhao et al., (2024) reported agriculture emission reductions since 2016, after the increase from 2011 to 2016, associated with the drying trend in South China and the transition from double-season to single-season rice cropping.

Waste represents the second-largest source of methane emissions in the study region, with posterior emissions of 28.76 Tg $yr^{-1}$ (24.99–34.41 Tg $yr^{-1}$). Major contributors include China, India, Indonesia, Pakistan, Thailand, the Philippines and Malaysia, where statistically significant increasing trends are consistently observed (Figure 6). The increase in waste-related methane emissions in developing countries is driven not only by rapid economic growth and urbanization, particularly in South Asia, but also by population growth, a high organic fraction of municipal solid waste, and the prevalence of unmanaged disposal practices and limited landfill gas recovery (Zhang et al., 2024). In addition, insufficient wastewater treatment coverage enhances methane generation (Toha et al., 2025). In Malaysia, emissions from wastewater treatment and discharge represent the dominant source within the waste sector, with industrial wastewater also contributing substantially, particularly wastewater treatment associated with palm oil mill effluent (Malaysia, 2022). Japan exhibits a significant decreasing trend, primarily attributable to long-standing regulatory frameworks that promote waste-to-energy utilization and high levels of recycling and reuse. Approximately 80% of combustible waste is incinerated with energy recovery, resulting in one of the world's lowest landfill usage rates at around 1% (Moshkal et al., 2024). Japan's experience in waste management provides valuable insights for achieving the sustainable development goals in developing countries, particularly through the adoption of advanced waste treatment technologies, strengthened waste reduction and recycling efforts, and enhanced environmental awareness.

Rapid economic growth and population growth have substantially increased regional energy demand, with most of this demand met by expanded use of fossil fuel (IEA, 2024). Consequently, the production and consumption of coal, oil and natural gas have continued to increase. Total coal emissions are estimated at 21.57 Tg $yr^{-1}$ (19.29–28.35 Tg $yr^{-1}$), with China contributing 62% and Indonesia 26% of regional emissions. The major coal producing and consuming countries, including China, Indonesia, Vietnam, Mongolia, all exhibit statistically significant increasing trends of coal emissions. In Indonesia, mean posterior coal emissions increased nearly fourfold from 2.02 to 7.94 Tg $yr^{-1}$ between 2010 and 2021, while emissions in Mongolia approximately doubled from 0.29 to 0.52 Tg $yr^{-1}$ over the same period (Our World in Data, 2024a). Total oil and natural gas emissions are estimated at 11.61 Tg $yr^{-1}$ (10.84–13.10 Tg $yr^{-1}$). In Malaysia, oil and gas emissions are estimated at 0.95 (0.85-1.05) Tg $yr^{-1}$, accounting for 54% of total anthropogenic emissions and show no statistically significant trend over the study period. In China, the increasing trends in coal and natural gas emissions are consistent with recent top-down estimates reported by Zhao et al. (2024). In contrast, oil and natural gas emissions in Indonesia, Vietnam, and Thailand display statistically significant decreasing trends. These declines across South Asia and Southeast Asia are likely associated with multiple factors, including the maturation and natural production

https://doi.org/10.5194/essd-2026-420
Preprint. Discussion started: 21 September 2026


decline of long-producing oil and gas fields—particularly in Indonesia and Malaysia, where production began in the 1970s and 1980s—as well as changes in global oil market conditions, such as increased production from North American shale resources, which have reduced oil prices and investment incentives for oil and gas development in Southeast Asia (IEA, 2024).

The total wetland emissions for the study area are estimated at 30.97 Tg $yr^{-1}$ (27.41 –35.06) Tg $yr^{-1}$, with Indonesia (10.75 Tg $yr^{-1}$) and India (6.08 Tg $yr^{-1}$) identified as the primary contributors. In several Southeast Asian nations —specifically Malaysia, Cambodia, Thailand, Vietnam, the Philippines, and Myanmar—estimated wetland emissions exceed 1 Tg $yr^{-1}$. Notably, in Indonesia and Malaysia, these emissions account for more than 50% of the total emissions (Figure 6). While significant increasing trends were observed in Vietnam and China, no statistically significant trends were detected in the remaining countries.

https://doi.org/10.5194/essd-2026-420
Preprint. Discussion started: 21 September 2026


Open Access Earth System Science Data Discussions

406 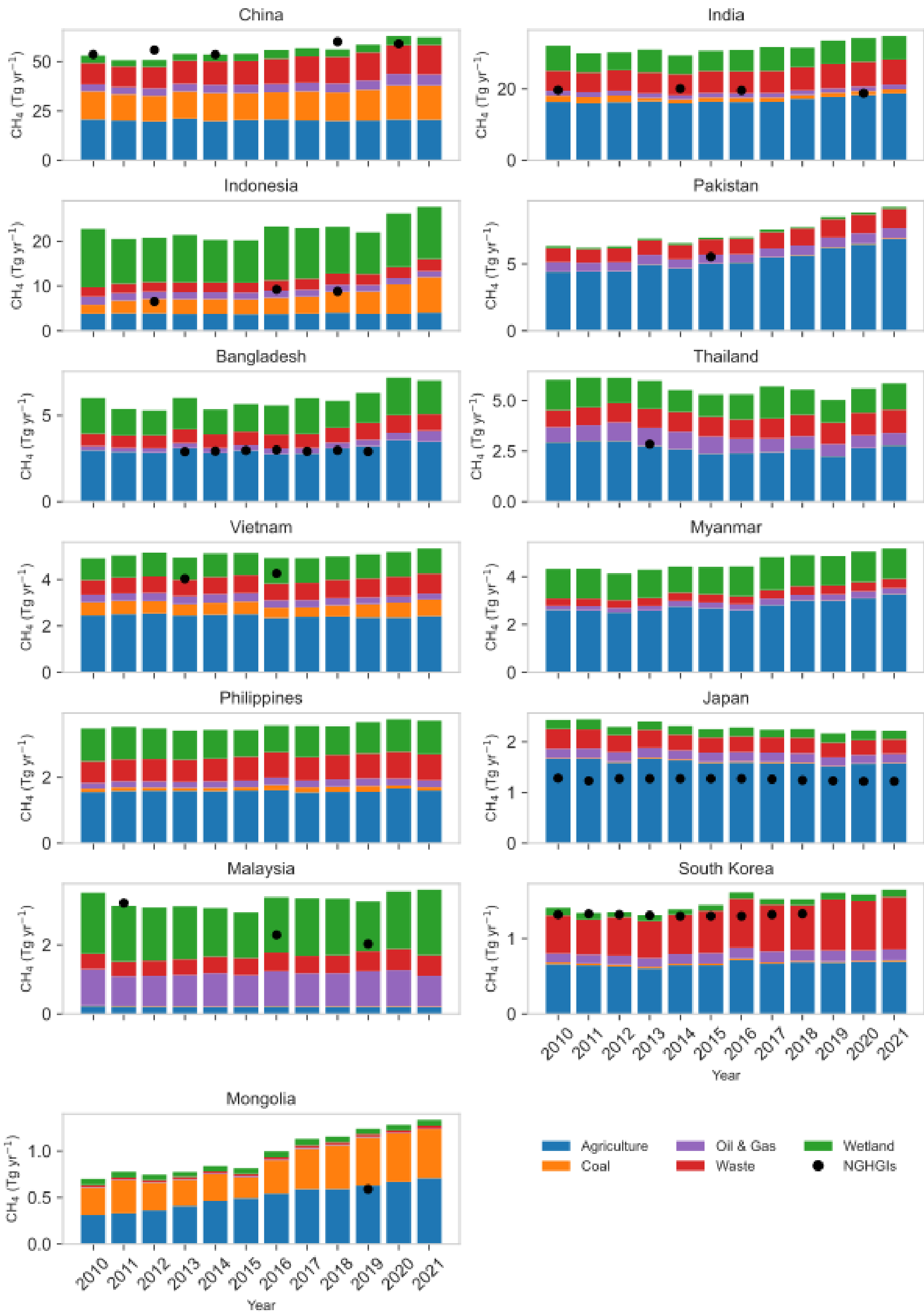


407 **Figure 6:** Posterior country-level sectoral emission trends for the period 2010–2021 for large emitting countries. UNFCCC
408 portal value available at https://di.unfccc.int/detailed_ data_by_party, and the more countries' Biennial Update Reports
409 (BURs) and National Communications (NCs) available at https://unfccc.int/BURs.

https://doi.org/10.5194/essd-2026-420
Preprint. Discussion started: 21 September 2026


Open Access Earth System Science Data Discussions

## 4 Discussions: Inter-model Differences

### 4.1 Model Performance Evaluation with Observations

To evaluate the performance of the inversion models, we compared simulated atmospheric concentrations derived from both prior and posterior emissions with optimized and independent observational datasets. The validation stations include two balloon-borne measurement sites in China and selected surface observations that are not assimilated in the inversions, as shown in Figure 1. We assessed model performance using standard statistical metrics, specifically mean bias, and root-mean-square error (RMSE), to quantify agreement between simulated and observed $CH_4$ concentrations. Figure 7 presents the model–data comparison at the sites used in inversion. Across all models, RMSEs estimated using posterior fluxes are significantly reduced compared to those using prior fluxes, indicating improved agreement with observations. The RMSE reductions exceed 50% for ACTM, LMDZ, NTLB, and CTE-CH4, while other models show more moderate improvements. Mean biases also decrease substantially from prior to posterior simulations. All models exhibit positive biases with prior fluxes, suggesting a systematic overestimation of atmospheric concentrations. After optimization, the biases are notably smaller and more variable in sign. NTFVAR, ACTM, and NTLB maintain small positive biases (less than +10 ppb), whereas GEOS-Chem, CTE-CH4, NTFVAR2, and LMDZ display negative biases. Among them, LMDZ shows the largest negative bias, with values below -10 ppb.

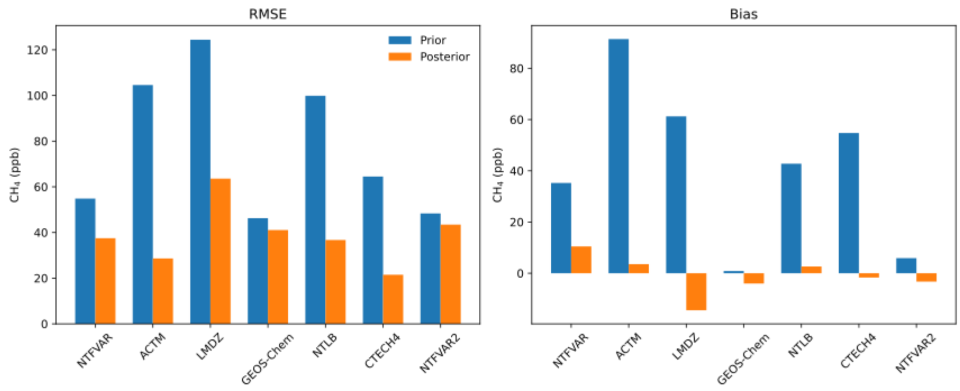


**Figure 7:** Average RMSE and mean bias for model simulations using prior and posterior fluxes at the stations used in SURF inversions.

Figure 8 compares the concentrations at surface validation sites (excluding balloon observations), illustrating the mean biases and RMSEs for SURF and GOS simulations. While RMSEs decrease from prior to posterior fluxes across all models, the reductions are generally smaller than those observed at the inversion stations. After optimization, RMSEs at validation sites remain relatively high, ranging from 30 to 60 ppb. Bias reductions are more pronounced, with most models exhibiting mean posterior biases below ±10 ppb. The LMDZ model is a notable exception, retaining a substantial negative bias of approximately 40–50 ppb. Overall, these comparisons demonstrate consistent improvements in model performance from prior to posterior simulations and underscore the consistency of posterior fluxes with independent atmospheric observations.

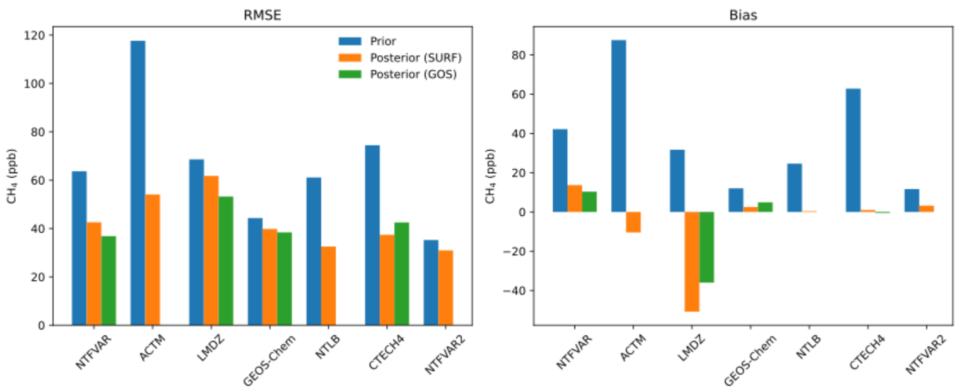


**Figure 8:** Average RMSE and mean bias for model simulations using prior and posterior fluxes at validation sites.

We also used balloon-borne observations to evaluate the ability of models to simulate vertical $CH_4$ profiles. Figure 9 presents the results from CTE-CH4, MIROC4-ACTM, and NTFVAR models. The observed vertical profile exhibits two distinct regimes: a relatively constant concentration of approximately 1900 ppb is maintained across the free troposphere (from approximately 700 to 200 hPa at site NMG and 600 to 100 hPa at site DCD), following a slight concentration decrease from the near-surface layer, and a sharp decline in concentration is observed in the upper troposphere and lower stratosphere region, corresponding to lower pressures zones. Simulated profiles derived from the posterior fluxes align much more closely with the observations than those derived from the prior fluxes. This improved performance is consistent across all three models, which generally maintain more constant concentrations throughout the free troposphere. However, particularly where the observed concentrations sharply decreases. The model simulations begin to diverge at higher altitudes. This discrepancy suggests that the effectiveness of the flux optimization in this region is limited by structural constraints in atmospheric transport models, particularly around the turning point in the concentration profile. Station DCD is located on the Tibetan Plateau at an altitude of approximately 4000 m, which may contribute to the greater variability observed in its vertical profile data.

https://doi.org/10.5194/essd-2026-420
Preprint. Discussion started: 21 September 2026


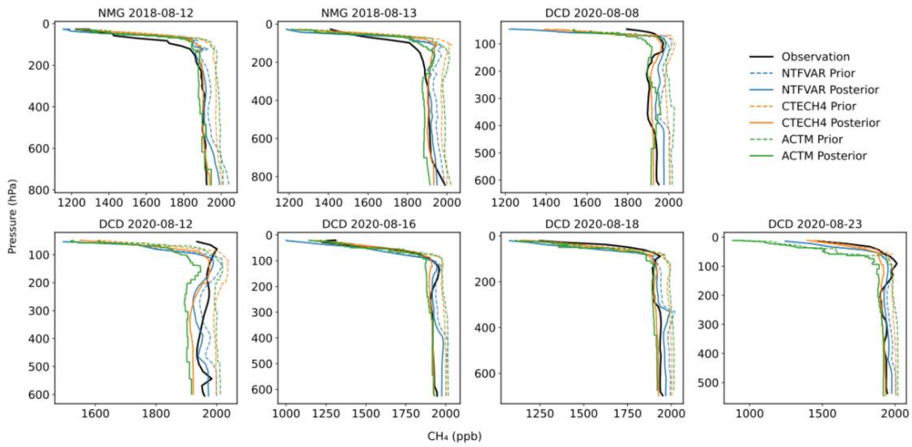


**Figure 9:** Comparison of observed and simulated vertical concentration profiles. The black lines denote the in-situ balloon observations (plotted at 1-minute temporal resolution). The dashed and solid colored lines represent the prior and posterior vertical profiles, respectively, simulated by three transport models: NTFVAR (blue), CTE-CH4 (orange), and MIROC4-ACTM (green).

### 4.2 Inter-model Spread in National Emission Estimates

The models participating in the MICA projects differ in horizontal resolutions and transport configurations, leading to measurable differences in prior emission estimates (Figure 3). Quantifying the spread introduced by the transport models themselves, independent of the underlying emission inventories, is essential for interpreting multi-model inversion results.

To characterize this inter-model spread, we employ the coefficient of variation (CV) and interquartile range (IQR) of national prior total emissions. Figure 10 presents the relationship between the CV and three-year mean prior emission totals, thereby minimizing the influence of seasonal and interannual variability. In most countries, the CV remains below 30%, with a median value of approximately 10%, indicating a moderate level of agreement across the ensemble. A small number of countries show exceptionally large CV values (>80%); however, these cases are primarily associated with very low national totals and small land areas, rather than fundamental model disagreement. The generally small IQR relative to the multi-model mean further suggests that the ensemble statistics are robust and not unduly influenced by individual models. The inter-model CV displays a systematic dependence on emission magnitude, with lower CV values for large-emitting countries and higher relative spread for small-emitting countries. This trend reflects the increased sensitivity of relative uncertainty metrics to model formulation and spatial aggregation at lower emission levels.

The impact of model granularity becomes evident when partitioning the ensemble by horizontal resolution. Models are categorized into two groups: coarse-resolution, including LMDZ (2.5° × 1.27°), CTE-CH4 (3° × 2°, 1° × 1° over high northern latitudes and Asia), and MIROC4-ACTM (2.8° × 2.8°), and higher-resolution

https://doi.org/10.5194/essd-2026-420
Preprint. Discussion started: 21 September 2026


comprising GEOS-Chem (0.5° × 0.625°), NTLB (0.5° × 0.5°), and NTFVAR (0.1° × 0.1°). The coarse-resolution group yields a higher mean CV (17.7%) and a significantly broader IQR (median = 10.7%; 75th percentile = 20.5%). Conversely, high-resolution models demonstrate much tighter agreement, with a lower mean CV (15.5%) and a smaller median IQR of only 3.2%. These findings underscore that horizontal resolution is a primary driver of inter-model spread in national emission estimates, persisting even when identical prior inventories are prescribed.

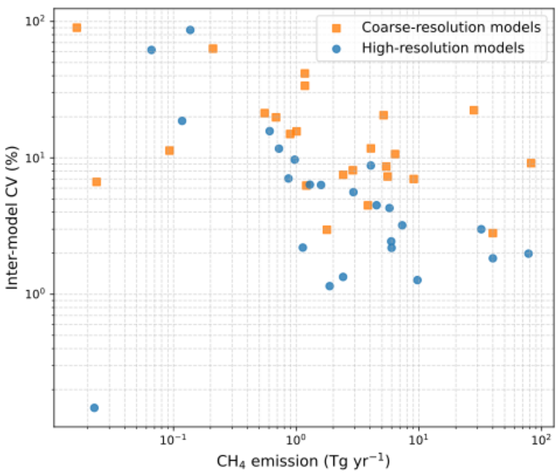


**Figure 10:** Inter-model variability (coefficient of variation, CV) versus national total $CH_4$ emissions derived from multiple inversion models. For each country, CV is computed across models using 3-year (2019-2021) mean emissions. Models are separated into high-resolution (blue circles) and coarse-resolution (orange squares) groups.

### 4.3 Consistency of Two Prior Emission Inventories

Within the MICA intercomparison framework, we examine the impact of prior inventory selection by comparing NTFVAR (which uses the standard MICA common prior) and NTFVAR2 (adopting an earlier version of the GCP prior). The Concordance Correlation Coefficient (CCC) (Lin, 1989) was used to evaluate reproducibility by measuring how well the two sets of national prior total emissions align with the 45-degree line of perfect agreement. The results show exceptional overall agreement (CCC = 0.9904) suggesting that the broad spatial distribution of methane sources remains consistent across the priors. However, a Bland-Altman analysis (Martin Bland and Altman, 1986) reveals localized divergences masked by this regional correlation. The most significant discrepancies, quantified by the Relative Percentage Difference (RPD), occur in nations such as East Timor (73.5%), Sri Lanka (37.9%), Afghanistan (35.3%), Bhutan (30.5%), and Bangladesh (19.7% RPD), which is a major emitter (~6.9 Tg $yr^{-1}$), likely because wetland emissions in the earlier GCP version differ significantly from the common MICA prior in these countries.

Sectoral emission trends also vary. In South Asia, NTFVAR shows a sharp increase in coal emissions that is absent in NTFVAR2. This discrepancy arises because NTFVAR2 relies on EDGAR v6, which only provides

https://doi.org/10.5194/essd-2026-420
Preprint. Discussion started: 21 September 2026


data through 2018; consequently, its coal emissions remain constant for 2018–2021, damping the inferred growth. Substantial differences exist in the oil and gas sector. NTFVAR2 employs the GAINS oil and gas prior instead of EDGAR v7 (Janardanan et al., 2024), resulting in emission estimates for Asia that are less than half of those in EDGAR-based priors over the 2010–2021 period. These differing priors drive the large spread in coal emissions for Indonesia and Vietnam, as well as the wide range of oil and gas sector across most countries for both prior and posterior emissions. These findings underscore that while regional prior totals may align, the specific inventory version significantly alters the 'starting point' for national-level inversions.

## 5 Data availability

The intercomparison protocol and the output database are available via Zenodo at https://doi.org/10.5281/zenodo.22699291 (Wang et al., 2026). The dataset includes NetCDF and CSV files, accompanied by documentations. These files provide: Monthly spatially resolved total and sectoral emissions (grid_[exp]_[model].nc); Integrated national, regional, and sectoral emission summaries aggregated across model groups (emis_[exp]_[model].csv/.nc); Ensemble-derived concentrations (conc_[exp]_[model].csv); Simulated concentrations sampled for independent validation data (val_[exp]_[model].csv).

To support ease of use, a complete usage example is documented via the Case Study: Interannual and Sectoral Variations in Asian Methane Emissions. Accompanying Python script is provided in the repository to read model outputs, handle temporal aggregation, compute robust ensemble statistics (medians and min-max spreads), evaluate long-term trends via the Mann-Kendall test, and automatically generate publication-ready boxplots, time-series plots, and summary text files.

The GOSAT data used in this study were obtained from the GOSAT Data Archive Service at the National Institute for Environmental Studies (NIES) (https://data2.gosat.nies.go.jp/). Additionally, $CH_4$ observation dataset were archived from the World Data Centre for Greenhouse Gases (WDCGG) (https://gaw.kishou.go.jp/) and the NOAA Global Monitoring Laboratory Obspack dataset (https://gml.noaa.gov/ccgg/obspack/).

## 6 Conclusions

This study presents the first coordinated multi-model, multi-group inversion intercomparison focused on $CH_4$ emissions over Asia, conducted under the Methane Inversion inter-Comparison for the Asian region (MICA) framework. By applying a standardized protocol with common prior fluxes, observational constraints, and validation datasets, MICA enables a consistent and quantitative evaluation of regional, national, and sectoral methane emission estimates for the 2010–2021 period, and provides an integrated dataset.

Across all models, inverse optimization results in a systematic reduction of total methane emissions relative to prior inventories. Averaged over Asia, posterior emissions decrease by approximately 15%, with the strongest reduction in East Asia (−25.8%), followed by South Asia (−10.4%) and Southeast Asia (−6.4%). Inter-model spread is reduced for the full domain, East Asia, and Southeast Asia, indicating improved ensemble convergence

https://doi.org/10.5194/essd-2026-420
Preprint. Discussion started: 21 September 2026




after optimization, while South Asia retains relatively large posterior uncertainty, reflecting limited observational constraints in this region. Mann–Kendall tests reveal statistically significant increasing trends ($p < 0.05$) in prior emissions across the full domain and all subregions, and these trends are largely preserved in the posterior estimates, indicating that inverse modeling primarily adjusts emission magnitudes rather than long-term growth. Comparisons between surface-only (SURF) and satellite-only (GOS) inversions show that observational constraints exert a strong influence on inferred emissions. GOS infers significantly higher emissions in East Asia and Southeast Asia relative to SURF, consistent with the reduced sensitivity of satellite column retrievals to local surface fluxes and their susceptibility to retrieval biases.

At the national scale, our analysis focuses on 13 “top-emitting” Asian countries; posterior total medians are consistently lower than their corresponding prior medians. China exhibits the largest downward corrections, with emissions reduced by 16% to the posterior median of to 64.88 Tg $yr^{-1}$, consistent with previous studies of overestimation in EDGAR-based inventories. Downward corrections of approximately 10% are also found for South Korea. Sectoral results reveal pronounced and systematic biases. Agriculture dominates methane emissions across Asia, with posterior emissions of 64.69 Tg $yr^{-1}$ (62.16–69.94 Tg $yr^{-1}$), contributing more than 50% of total anthropogenic emissions in most countries. Statistically significant increasing trends are observed in India, Pakistan, Myanmar, and Mongolia, consistent with expanding rice cultivation and livestock populations, while Japan and Malaysia exhibit decreasing agricultural emissions. Waste is the second-largest source, with posterior emissions of 28.76 Tg $yr^{-1}$ (24.99–34.41 Tg $yr^{-1}$), and shows widespread increasing trends in major emitting countries. Coal-related emissions total 21.57 Tg $yr^{-1}$ (19.29–28.35 Tg $yr^{-1}$), with strong upward corrections in Mongolia (+70%) and Pakistan (+50%), and major downward corrections in China (−30%) and Malaysia (−33%). Oil and natural gas emissions are estimated at 11.61 Tg $yr^{-1}$ (10.84–13.10 Tg $yr^{-1}$), with heterogeneous national trends, including stable emissions in Malaysia and declining emissions in parts of Southeast Asia. Wetland emissions are estimated at 30.97 Tg $yr^{-1}$ (27.41–35.06) Tg $yr^{-1}$, mainly from Southeast countries.

Evaluation against surface, aircraft, and balloon-borne observations demonstrates substantial improvements in simulated methane concentrations after optimization. RMSEs decrease by more than 50% for several models, and mean biases are reduced to within approximately ±10 ppb. Nevertheless, posterior RMSEs at independent validation sites remain relatively high (30–60 ppb), highlighting the future need for denser and more regionally representative observational networks, particularly in South Asia and Southeast Asia. Inter-model uncertainty shows a strong dependence on model horizontal resolution. Coarse-resolution models exhibit larger relative spread (mean CV 17.7%) than higher-resolution models (mean CV 15.5%, median IQR 3.2%), even when identical priors are prescribed. In contrast, differences arising from alternative versions of global prior inventories are generally modest at regional and national scales (CV ≈ 5–10% for major emitters), though sectoral discrepancies, especially for coal and oil and gas, remain substantial. Although there are systemic biases in prior inventories, our anlysis highlighting Southeast Asian waste and energy-sector emissions require urgent validation through densified observation networks.

In this study, we demonstrate the implications of the MICA dataset by analyzing national and sectoral emissions. The results from the MICA intercomparison reveal that a multi-model ensemble approach improves

https://doi.org/10.5194/essd-2026-420
Preprint. Discussion started: 21 September 2026


the consistency and transparency of Asian CH4 emission estimates. This intercomparison establishes a robust baseline, facilitating the integration of observational constraints into national emission inventories to support reporting and evaluate emission reduction progress and track climate policy effectiveness. Furthermore, the dataset can be used for distinguishing emission contributions across sectors, helping policymakers target high-emitting areas. It provides transparent, independent scientific support to the global stocktake. It also serves as a methodological benchmark for reasearch, providing a the multi-model ensemble framework and outputs that assist researchers in conducting independent inversee modeling, model development, and performance assessments. Additionally, we provide practical examples in the dataset documentation for researchers interested in conducting their own analysis. However, we note that due to limitations in spatial resolution and sparse observations, the dataset can not resolve fine-scale emissions within individal cities or small countries. It is not suitable for locating or quantifying specific point sources, which require high-resolution satellite imagery or targeted in-situ measurements. Due to sparse observaitonal constrains and smoothing effects in inversions, the dataset is best suited for long-term trend or interannual variability analysis rather than capturing high-frequency temporal dyanamics, such as diurnal or hourly variations.

**Competing interests**

The contact author has declared that none of the authors has any competing interests.

**Author contributions**

FW and SM coordinated this inter-comparison as part of the NIES GOSAT project and developed the study protocol. FW led the integated analysis, performed the NTFVAR inversions, and drafted the manuscript. Model simulations and output were provided by RJ (NTFVAR2), DB and PP (MIROC4-ACTM), RL and YZ (GEOS-Chem), GR and HL (NTLB), NM, AB, MS, and AM (LMDZ), and SH and AT (CTE-CH4). ML, XL, YT, MKA, and MN contributed to observation data. IM, YY, YS, TS and TM contributed to GOSAT data, and AI provided VISIT data. All co-authors participated in the discussion of the results and contributed to the revision of the manuscript.

**Acknowledgements**

We acknowledge the Ministry of the Environment, Japan, for its financial support of the GOSAT series projects, including inverse model development and GHG emissions analysis. We extend our thanks to the institutions that contributed observational data through the Obspack dataset, the World Data Centre for Greenhouse Gases (WDCGG), and NIES. We also thank Mr. Daegeun Shin from the National Institute of Meteorological Sciences, Republic of Korea, for providing observational data from the ULD site. Financial support from the European Space Agency is acknowledged under ESRIN Contract No: 4000137895/22/I-AG MethaneCAMP, AO/1-10901/21/I-DT AMPAC-Net, ESA AO/1-11844/23/I-NS ESA SMART-CH4. Support from ANID through the PhD fellowship “ANID BECAS/DOCTORADO EN EL EXTRANJERO (Becas Chile)” No. 72220111 and from CNES through doctoral fellowship No. 5100020500 is gratefully acknowledged. We acknowledge funding from the Research Council of Finland projects 337552 (ACCC), 359196 (FAME) and 364975 (CHARM), PeatResC (374130), FIRI - ICOS Finland (345531) and EU Horizon IM4CA (101183460). We also acknowledge the use of ChatGPT (OpenAI), Copilot (Microsoft) and Gemini (Google) for assistance in developing programming scripts used for data analysis and visualization.

**References**

Belikov, D. A., Maksyutov, S., Yaremchuk, A., Ganshin, A., Kaminski, T., Blessing, S., Sasakawa, M., Gomez-Pelaez, A. J., and Starchenko, A.: Adjoint of the global Eulerian–Lagrangian coupled atmospheric transport model (A-GELCA v1.0): development and validation, Geosci. Model Dev., 9, 749–764, https://doi.org/10.5194/gmd-9-749-2016, 2016.

Belikov, D. A., Patra, P. K., Terao, Y., Naja, M., Ahmed, Md. K., and Saitoh, N.: Assessment of the impact of observations at Nainital (India) and Comilla (Bangladesh) on the CH4 flux inversion, Prog. Earth Planet. Sci., 11, 36, https://doi.org/10.1186/s40645-024-00634-x, 2024.

Berchet, A., Sollum, E., Thompson, R. L., Pison, I., Thanwerdas, J., Broquet, G., Chevallier, F., Aalto, T., Berchet, A., Bergamaschi, P., Brunner, D., Engelen, R., Fortems-Cheiney, A., Gerbig, C., Groot Zwaaftink, C. D., Haussaire, J.-M., Henne, S., Houweling, S., Karstens, U., Kutsch, W. L., Luijkx, I. T., Monteil, G., Palmer, P. I., Van Peet, J. C. A., Peters, W., Peylin, P., Potier, E., Rödenbeck, C., Saunois, M., Scholze, M., Tsuruta, A., and Zhao, Y.: The Community Inversion Framework v1.0: a unified system for atmospheric inversion studies, Geosci. Model Dev., 14, 5331–5354, https://doi.org/10.5194/gmd-14-5331-2021, 2021.

Bruhwiler, L., Dlugokencky, E., Masarie, K., Ishizawa, M., Andrews, A., Miller, J., Sweeney, C., Tans, P., and Worthy, D.: CarbonTracker-$CH_4$ : an assimilation system for estimating emissions of atmospheric methane, Atmospheric Chem. Phys., 14, 8269–8293, https://doi.org/10.5194/acp-14-8269-2014, 2014.

Chandra, N., Patra, P. K., Bisht, J. S. H., Ito, A., Umezawa, T., Saigusa, N., Morimoto, S., Aoki, S., Janssens-Maenhout, G., Fujita, R., Takigawa, M., Watanabe, S., Saitoh, N., and Canadell, J. G.: Emissions from the Oil and Gas Sectors, Coal Mining and Ruminant Farming Drive Methane Growth over the Past Three Decades, J. Meteorol. Soc. Jpn. Ser II, 99, 309–337, https://doi.org/10.2151/jmsj.2021-015, 2021.

Chiao, L., Fang, H., Gung, Y., Chang, Y., and Hung, S.: Comparative appraisal of linear inverse models constructed via distinctive parameterizations (comparing distinctly inverted models), J. Geophys. Res. Solid Earth, 115, 2009JB006867, https://doi.org/10.1029/2009JB006867, 2010.

Crippa, M., Guizzardi, D., Solazzo, E., Muntean, M., Schaaf, E., Monforti-Ferrario, F., Banja, M., Oliver, J. G. J., Grassi, G., and Vignati, E.: GHG emissions of all world: 2021 report., https://doi.org/10.2760/173513, 2021.

Deng, Z., Ciais, P., Hu, L., Martinez, A., Saunois, M., Thompson, R. L., Tibrewal, K., Peters, W., Byrne, B., Grassi, G., Palmer, P. I., Luijkx, I. T., Liu, Z., Liu, J., Fang, X., Wang, T., Tian, H., Tanaka, K., Bastos, A., Sitch, S., Poulter, B., Albergel, C., Tsuruta, A., Maksyutov, S., Janardanan, R., Niwa, Y., Zheng, B., Thanwerdas, J., Belikov, D., Segers, A., and Chevallier, F.: Global greenhouse gas reconciliation 2022, Earth Syst. Sci. Data, 17, 1121–1152, https://doi.org/10.5194/essd-17-1121-2025, 2025.

Dlugokencky, E. J., Masarie, K. A., Lang, P. M., and Tans, P. P.: Continuing decline in the growth rate of the atmospheric methane burden, Nature, 393, 447–450, https://doi.org/10.1038/30934, 1998.

Dlugokencky, E. J., Houweling, S., Bruhwiler, L., Masarie, K. A., Lang, P. M., Miller, J. B., and Tans, P. P.: Atmospheric methane levels off: Temporary pause or a new steady-state?, Geophys. Res. Lett., 30, 2003GL018126, https://doi.org/10.1029/2003GL018126, 2003.

Dlugokencky, E. J., Bruhwiler, L., White, J. W. C., Emmons, L. K., Novelli, P. C., Montzka, S. A., Masarie, K. A., Lang, P. M., Crotwell, A. M., Miller, J. B., and Gatti, L. V.: Observational constraints on recent increases in the atmospheric $CH_4$ burden, Geophys. Res. Lett., 36, 2009GL039780, https://doi.org/10.1029/2009GL039780, 2009.

Dlugokencky, E. J., Nisbet, E. G., Fisher, R., and Lowry, D.: Global atmospheric methane: budget, changes and dangers, Philos. Trans. R. Soc. Math. Phys. Eng. Sci., 369, 2058–2072, https://doi.org/10.1098/rsta.2010.0341, 2011.

https://doi.org/10.5194/essd-2026-420
Preprint. Discussion started: 21 September 2026


East, J. D., Jacob, D. J., Jervis, D., Balasus, N., Estrada, L. A., Hancock, S. E., Sulprizio, M. P., Thomas, J., Wang, X., Chen, Z., Varon, D. J., and Worden, J. R.: Worldwide inference of national methane emissions by inversion of satellite observations with UNFCCC prior estimates, Nat. Commun., 16, 11004, https://doi.org/10.1038/s41467-025-67122-8, 2025.

Etheridge, D. M., Steele, L. P., Francey, R. J., and Langenfelds, R. L.: Atmospheric methane between 1000 A.D. and present: Evidence of anthropogenic emissions and climatic variability, J. Geophys. Res. Atmospheres, 103, 15979–15993, https://doi.org/10.1029/98JD00923, 1998.

Etiope, G., Ciotoli, G., Schwietzke, S., and Schoell, M.: Gridded maps of geological methane emissions and their isotopic signature, Earth Syst. Sci. Data, 11, 1–22, https://doi.org/10.5194/essd-11-1-2019, 2019.

Fletcher, S. E. M. and Schaefer, H.: Rising methane: A new climate challenge, Science, 364, 932–933, https://doi.org/10.1126/science.aax1828, 2019.

Gelaro, R., McCarty, W., Suárez, M. J., Todling, R., Molod, A., Takacs, L., Randles, C. A., Darmenov, A., Bosilovich, M. G., Reichle, R., Wargan, K., Coy, L., Cullather, R., Draper, C., Akella, S., Buchard, V., Conaty, A., Da Silva, A. M., Gu, W., Kim, G.-K., Koster, R., Lucchesi, R., Merkova, D., Nielsen, J. E., Partyka, G., Pawson, S., Putman, W., Rienecker, M., Schubert, S. D., Sienkiewicz, M., and Zhao, B.: The Modern-Era Retrospective Analysis for Research and Applications, Version 2 (MERRA-2), J. Clim., 30, 5419–5454, https://doi.org/10.1175/JCLI-D-16-0758.1, 2017.

Gilbert, R. O.: Statistical Methods for Environmental Pollution Monitoring., Biometrics, 44, 319, https://doi.org/10.2307/2531935, 1988.

Grell, G. A., Peckham, S. E., Schmitz, R., McKeen, S. A., Frost, G., Skamarock, W. C., and Eder, B.: Fully coupled "online" chemistry within the WRF model, Atmos. Environ., 39, 6957–6975, https://doi.org/10.1016/j.atmosenv.2005.04.027, 2005.

Hourdin, F., Musat, I., Bony, S., Braconnot, P., Codron, F., Dufresne, J.-L., Fairhead, L., Filiberti, M.-A., Friedlingstein, P., Grandpeix, J.-Y., Krinner, G., LeVan, P., Li, Z.-X., and Lott, F.: The LMDZ4 general circulation model: climate performance and sensitivity to parametrized physics with emphasis on tropical convection, Clim. Dyn., 27, 787–813, https://doi.org/10.1007/s00382-006-0158-0, 2006.

Houweling, S., Baker, D., Basu, S., Boesch, H., Butz, A., Chevallier, F., Deng, F., Dlugokencky, E. J., Feng, L., Ganshin, A., Hasekamp, O., Jones, D., Maksyutov, S., Marshall, J., Oda, T., O'Dell, C. W., Oshchepkov, S., Palmer, P. I., Peylin, P., Poussi, Z., Reum, F., Takagi, H., Yoshida, Y., and Zhuravlev, R.: An intercomparison of inverse models for estimating sources and sinks of $CO_2$ using GOSAT measurements, J. Geophys. Res. Atmospheres, 120, 5253–5266, https://doi.org/10.1002/2014JD022962, 2015.

Houweling, S., Bergamaschi, P., Chevallier, F., Heimann, M., Kaminski, T., Krol, M., Michalak, A. M., and Patra, P.: Global inverse modeling of $CH_4$ sources and sinks: an overview of methods, Atmospheric Chem. Phys., 17, 235–256, https://doi.org/10.5194/acp-17-235-2017, 2017.

Hu, H., Hasekamp, O., Butz, A., Galli, A., Landgraf, J., Aan De Brugh, J., Borsdorff, T., Scheepmaker, R., and Aben, I.: The operational methane retrieval algorithm for TROPOMI, Atmospheric Meas. Tech., 9, 5423–5440, https://doi.org/10.5194/amt-9-5423-2016, 2016.

IEA: The Southeast Asia Energy Outlook 2024, https://iea.blob.core.windows.net/assets/ac357b64-0020-421c-98d7-f5c468dadb0f/SoutheastAsiaEnergyOutlook2024.pdf, 2024.

Ioannidis, E., Meesters, A., Steiner, M., Brunner, D., Reum, F., Pison, I., Berchet, A., Thompson, R., Sollum, E., Koch, F.-T., Gerbig, C., Wang, F., Maksyutov, S., Tsuruta, A., Tenkanen, M., Aalto, T., Monteil, G., Lin, H., Ren, G., Scholze, M., and Houweling, S.: An inter-comparison of inverse models for estimating European $CH_4$ emissions, Earth Syst. Sci. Data, 18, 167–198, https://doi.org/10.5194/essd-18-167-2026, 2026.

IPCC: Climate Change 2021 – The Physical Science Basis: Working Group I Contribution to the Sixth Assessment Report of the Intergovernmental Panel on Climate Change, 1st ed., Cambridge University Press, https://doi.org/10.1017/9781009157896, 2023.

https://doi.org/10.5194/essd-2026-420
Preprint. Discussion started: 21 September 2026


Ito, A. and Inatomi, M.: Use of a process-based model for assessing the methane budgets of global terrestrial ecosystems and evaluation of uncertainty, Biogeosciences, 9, 759–773, https://doi.org/10.5194/bg-9-759-2012, 2012.

Ito, A., Tohjima, Y., Saito, T., Umezawa, T., Hajima, T., Hirata, R., Saito, M., and Terao, Y.: Methane budget of East Asia, 1990–2015: A bottom-up evaluation, Sci. Total Environ., 676, 40–52, https://doi.org/10.1016/j.scitotenv.2019.04.263, 2019.

Ito, A., Patra, P. K., and Umezawa, T.: Bottom-Up Evaluation of the Methane Budget in Asia and Its Subregions, Glob. Biogeochem. Cycles, 37, e2023GB007723, https://doi.org/10.1029/2023GB007723, 2023.

Jackson, R. B., Saunois, M., Martinez, A., Canadell, J. G., Yu, X., Li, M., Poulter, B., Raymond, P. A., Regnier, P., Ciais, P., Davis, S. J., and Patra, P. K.: Human activities now fuel two-thirds of global methane emissions, Environ. Res. Lett., 19, 101002, https://doi.org/10.1088/1748-9326/ad6463, 2024.

Jacob, D. J., Varon, D. J., Cusworth, D. H., Dennison, P. E., Frankenberg, C., Gautam, R., Guanter, L., Kelley, J., McKeever, J., Ott, L. E., Poulter, B., Qu, Z., Thorpe, A. K., Worden, J. R., and Duren, R. M.: Quantifying methane emissions from the global scale down to point sources using satellite observations of atmospheric methane, Atmospheric Chem. Phys., 22, 9617–9646, https://doi.org/10.5194/acp-22-9617-2022, 2022.

Janardanan, R., Maksyutov, S., Tsuruta, A., Wang, F., Tiwari, Y. K., Valsala, V., Ito, A., Yoshida, Y., Kaiser, J. W., Janssens-Maenhout, G., Arshinov, M., Sasakawa, M., Tohjima, Y., Worthy, D. E. J., Dlugokencky, E. J., Ramonet, M., Arduini, J., Lavric, J. V., Piacentino, S., Krummel, P. B., Langenfelds, R. L., Mammarella, I., and Matsunaga, T.: Country-Scale Analysis of Methane Emissions with a High-Resolution Inverse Model Using GOSAT and Surface Observations, Remote Sens., 12, 375, https://doi.org/10.3390/rs12030375, 2020.

Janardanan, R., Maksyutov, S., Wang, F., Nayagam, L., Sahu, S. K., Mangaraj, P., Saunois, M., Lan, X., and Matsunaga, T.: Country-level methane emissions and their sectoral trends during 2009–2020 estimated by high-resolution inversion of GOSAT and surface observations, Environ. Res. Lett., 19, 034007, https://doi.org/10.1088/1748-9326/ad2436, 2024.

Kaiser, J. W., Heil, A., Andreae, M. O., Benedetti, A., Chubarova, N., Jones, L., Morcrette, J.-J., Razinger, M., Schultz, M. G., Suttie, M., and Van Der Werf, G. R.: Biomass burning emissions estimated with a global fire assimilation system based on observed fire radiative power, https://doi.org/10.5194/bgd-8-7339-2011, 22 July 2011., 2011.

Kirschke, S., Bousquet, P., Ciais, P., Saunois, M., Canadell, J. G., Dlugokencky, E. J., Bergamaschi, P., Bergmann, D., Blake, D. R., Bruhwiler, L., Cameron-Smith, P., Castaldi, S., Chevallier, F., Feng, L., Fraser, A., Heimann, M., Hodson, E. L., Houweling, S., Josse, B., Fraser, P. J., Krummel, P. B., Lamarque, J.-F., Langenfelds, R. L., Le Quéré, C., Naik, V., O'Doherty, S., Palmer, P. I., Pison, I., Plummer, D., Poulter, B., Prinn, R. G., Rigby, M., Ringeval, B., Santini, M., Schmidt, M., Shindell, D. T., Simpson, I. J., Spahni, R., Steele, L. P., Strode, S. A., Sudo, K., Szopa, S., Van Der Werf, G. R., Voulgarakis, A., Van Weele, M., Weiss, R. F., Williams, J. E., and Zeng, G.: Three decades of global methane sources and sinks, Nat. Geosci., 6, 813–823, https://doi.org/10.1038/ngeo1955, 2013.

Kobayashi, S., Ota, Y., Harada, Y., Ebita, A., Moriya, M., Onoda, H., Onogi, K., Kamahori, H., Kobayashi, C., Endo, H., Miyaoka, K., and Takahashi, K.: The JRA-55 Reanalysis: General Specifications and Basic Characteristics, J. Meteorol. Soc. Jpn. Ser II, 93, 5–48, https://doi.org/10.2151/jmsj.2015-001, 2015.

Kondo, M., Patra, P. K., Canadell, J. G., Ciais, P., Houghton, R. A., Ito, A., Deshmukh, C. S., Kumagai, T., Luo, X., Mishra, U., Jain, A. K., Li, W., Koren, G., Sitch, S., Poulter, B., Tian, H., Bastos, A., Lauerwald, R., Rosentreter, J. A., Chandra, N., Saeki, T., Saunois, M., Luijkx, I. T., Maki, T., Nakamura, T., Hirabayashi, K., Hirano, T., and Saigusa, N.: The Greenhouse Gas Budget of Southeast Asia for 2000–2019 and Pathways Toward Climate Neutrality, Glob. Biogeochem. Cycles, 39, e2024GB008256, https://doi.org/10.1029/2024GB008256, 2025.

Krol, M., Houweling, S., Bregman, B., Van Den Broek, M., Segers, A., Van Velthoven, P., Peters, W., Dentener, F., and Bergamaschi, P.: The two-way nested global chemistry-transport zoom model TM5: algorithm and applications, Atmospheric Chem. Phys., 5, 417–432, https://doi.org/10.5194/acp-5-417-2005, 2005.

https://doi.org/10.5194/essd-2026-420
Preprint. Discussion started: 21 September 2026


Kuze, A., Suto, H., Nakajima, M., and Hamazaki, T.: Thermal and near infrared sensor for carbon observation Fourier-transform spectrometer on the Greenhouse Gases Observing Satellite for greenhouse gases monitoring, Appl. Opt., 48, 6716, https://doi.org/10.1364/AO.48.006716, 2009.

Lan, X., Thoning, K., and Dlugokencky, E.: Trends in globally-averaged CH4, N2O, and SF6 determined from NOAA Global Monitoring Laboratory, https://doi.org/10.15138/P8XG-AA10, 2022.

Liang, R., Zhang, Y., Chen, W., Zhang, P., Liu, J., Chen, C., Mao, H., Shen, G., Qu, Z., Chen, Z., Zhou, M., Wang, P., Parker, R. J., Boesch, H., Lorente, A., Maasakkers, J. D., and Aben, I.: East Asian methane emissions inferred from high-resolution inversions of GOSAT and TROPOMI observations: a comparative and evaluative analysis, Atmospheric Chem. Phys., 23, 8039–8057, https://doi.org/10.5194/acp-23-8039-2023, 2023.

Liang, R., Zhang, Y., Hu, Q., Li, T., Li, S., Yuan, W., Xu, J., Zhao, Y., Zhang, P., Chen, W., Zhuang, M., Shen, G., and Chen, Z.: Satellite-Based Monitoring of Methane Emissions from China's Rice Hub, Environ. Sci. Technol., 58, 23127–23137, https://doi.org/10.1021/acs.est.4c09822, 2024.

Lin, J. C., Gerbig, C., Wofsy, S. C., Andrews, A. E., Daube, B. C., Davis, K. J., and Grainger, C. A.: A near-field tool for simulating the upstream influence of atmospheric observations: The Stochastic Time-Inverted Lagrangian Transport (STILT) model, J. Geophys. Res. Atmospheres, 108, 2002JD003161, https://doi.org/10.1029/2002JD003161, 2003.

Lin, L. I.-K.: A Concordance Correlation Coefficient to Evaluate Reproducibility, Biometrics, 45, 255, https://doi.org/10.2307/2532051, 1989.

Maksyutov, S., Oda, T., Saito, M., Janardanan, R., Belikov, D., Kaiser, J. W., Zhuravlev, R., Ganshin, A., Valsala, V. K., Andrews, A., Chmura, L., Dlugokencky, E., Haszpra, L., Langenfelds, R. L., Machida, T., Nakazawa, T., Ramonet, M., Sweeney, C., and Worthy, D.: Technical note: A high-resolution inverse modelling technique for estimating surface $CO_2$ fluxes based on the NIES-TM–FLEXPART coupled transport model and its adjoint, Atmospheric Chem. Phys., 21, 1245–1266, https://doi.org/10.5194/acp-21-1245-2021, 2021.

Malaysia: Fourth Biennial Update Report under the United Nations Framework Convention on Climate Change, MINISTRY OF NATURAL RESOURCES, ENVIRONMENT AND CLIMATE CHANGE, MALAYSIA, Putrajaya, https://unfccc.int/sites/default/files/resource/MY%20BUR4_2022.pdf, 2022.

Marine Regions: Marineregions: intersect of EEZs and IHO areas (3), https://www.marineregions.org/downloads.php (last access: 17 July 2023), 2018.

Martin Bland, J. and Altman, DouglasG.: STATISTICAL METHODS FOR ASSESSING AGREEMENT BETWEEN TWO METHODS OF CLINICAL MEASUREMENT, The Lancet, 327, 307–310, https://doi.org/10.1016/S0140-6736(86)90837-8, 1986.

Monteil, G., Broquet, G., Scholze, M., Lang, M., Karstens, U., Gerbig, C., Koch, F.-T., Smith, N. E., Thompson, R. L., Luijkx, I. T., White, E., Meesters, A., Ciais, P., Ganesan, A. L., Manning, A., Mischurow, M., Peters, W., Peylin, P., Tarniewicz, J., Rigby, M., Rödenbeck, C., Vermeulen, A., and Walton, E. M.: The regional European atmospheric transport inversion comparison, EUROCOM: first results on European-wide terrestrial carbon fluxes for the period 2006–2015, Atmospheric Chem. Phys., 20, 12063–12091, https://doi.org/10.5194/acp-20-12063-2020, 2020.

Montenegro, N., Berchet, A., Martinez, A., Thanwerdas, J., Bousquet, P., Pison, I., and Saunois, M.: Capability of current observing systems to monitor $CH_4$ emissions from the regional to the global scales, https://doi.org/10.5194/egusphere-2025-5923, 23 December 2025., 2025.

Moshkal, M., Akhapov, Y., and Ogihara, A.: Sustainable Waste Management in Japan: Challenges, Achievements, and Future Prospects: A Review, Sustainability, 16, 7347, https://doi.org/10.3390/su16177347, 2024.

Nisbet, E. G., Dlugokencky, E. J., and Bousquet, P.: Methane on the Rise—Again, Science, 343, 493–495, https://doi.org/10.1126/science.1247828, 2014.

Nisbet, E. G., Dlugokencky, E. J., Manning, M. R., Lowry, D., Fisher, R. E., France, J. L., Michel, S. E., Miller, J. B., White, J. W. C., Vaughn, B., Bousquet, P., Pyle, J. A., Warwick, N. J., Cain, M., Brownlow, R., Zazzeri, G., Lanoisellé, M., Manning, A. C., Gloor, E., Worthy, D. E. J., Brunke, E. -G., Labuschagne, C., Wolff, E. W., and Ganesan, A. L.: Rising atmospheric methane: 2007–2014 growth and isotopic shift, Glob. Biogeochem. Cycles, 30, 1356–1370, https://doi.org/10.1002/2016GB005406, 2016.

Nisbet, E. G., Manning, M. R., Dlugokencky, E. J., Fisher, R. E., Lowry, D., Michel, S. E., Myhre, C. L., Platt, S. M., Allen, G., Bousquet, P., Brownlow, R., Cain, M., France, J. L., Hermansen, O., Hossaini, R., Jones, A. E., Levin, I., Manning, A. C., Myhre, G., Pyle, J. A., Vaughn, B. H., Warwick, N. J., and White, J. W. C.: Very Strong Atmospheric Methane Growth in the 4 Years 2014–2017: Implications for the Paris Agreement, Glob. Biogeochem. Cycles, 33, 318–342, https://doi.org/10.1029/2018GB006009, 2019.

Niwa, Y., Tohjima, Y., Terao, Y., Saeki, T., Ito, A., Umezawa, T., Yamada, K., Sasakawa, M., Machida, T., Nakaoka, S.-I., Nara, H., Tanimoto, H., Mukai, H., Yoshida, Y., Morimoto, S., Takatsuji, S., Tsuboi, K., Sawa, Y., Matsueda, H., Ishijima, K., Fujita, R., Goto, D., Lan, X., Schuldt, K., Heliasz, M., Biermann, T., Chmura, L., Necki, J., and Xueref-Remy, I.: Multi-observational estimation of regional and sectoral emission contributions to the persistent high growth rate of atmospheric $CH_4$ for 2020–2022, https://doi.org/10.5194/egusphere-2024-2457, 26 August 2024., 2024.

Nomura, S., Naja, M., Ahmed, M. K., Mukai, H., Terao, Y., Machida, T., Sasakawa, M., and Patra, P. K.: Measurement report: Regional characteristics of seasonal and long-term variations in greenhouse gases at Nainital, India, and Comilla, Bangladesh, Atmospheric Chem. Phys., 21, 16427–16452, https://doi.org/10.5194/acp-21-16427-2021, 2021.

O'Connor, F. M., Johnson, B. T., Jamil, O., Andrews, T., Mulcahy, J. P., and Manners, J.: Apportionment of the Pre-Industrial to Present-Day Climate Forcing by Methane Using UKESM1: The Role of the Cloud Radiative Effect, J. Adv. Model. Earth Syst., 14, e2022MS002991, https://doi.org/10.1029/2022MS002991, 2022.

Our World in Data: Coal production, https://ourworldindata.org/grapher/coal-production-by-country?country=GBR~USA~CHN~IND (last access: 9 January 2026a), 2024.

Our World in Data: Livestock Counts: Cattle, Sheep, and Goats, https://ourworldindata.org/grapher/cattle-livestock-count-heads (last access: 9 April 2026b), 2024.

Parker, R. and Boesch, H.: University of Leicester GOSAT Proxy XCH4 v9.0, https://doi.org/10.5285/18EF8247F52A4CB6A14013F8235CC1EB, 2020.

Patra, P. K., Saeki, T., Dlugokencky, E. J., Ishijima, K., Umezawa, T., Ito, A., Aoki, S., Morimoto, S., Kort, E. A., Crotwell, A., Ravi Kumar, K., and Nakazawa, T.: Regional Methane Emission Estimation Based on Observed Atmospheric Concentrations (2002-2012), J. Meteorol. Soc. Jpn. Ser II, 94, 91–113, https://doi.org/10.2151/jmsj.2016-006, 2016.

Patra, P. K., Takigawa, M., Watanabe, S., Chandra, N., Ishijima, K., and Yamashita, Y.: Improved Chemical Tracer Simulation by MIROC4.0-based Atmospheric Chemistry-Transport Model (MIROC4-ACTM), SOLA, 14, 91–96, https://doi.org/10.2151/sola.2018-016, 2018.

Peters, W., Miller, J. B., Whitaker, J., Denning, A. S., Hirsch, A., Krol, M. C., Zupanski, D., Bruhwiler, L., and Tans, P. P.: An ensemble data assimilation system to estimate $CO_2$ surface fluxes from atmospheric trace gas observations, J. Geophys. Res. Atmospheres, 110, 2005JD006157, https://doi.org/10.1029/2005JD006157, 2005.

Pison, I., Bousquet, P., Chevallier, F., Szopa, S., and Hauglustaine, D.: Multi-species inversion of $CH_4$, CO and $H_2$ emissions from surface measurements, Atmospheric Chem. Phys., 9, 5281–5297, https://doi.org/10.5194/acp-9-5281-2009, 2009.

Poulter, B., Murray-Tortarolo, G., Hayes, D. J., Ciais, P., Andrew, R. M., Bastos, A., Byrne, B., Butman, D., Canadell, J. G., Chatterjee, A., Domke, G., Feldman, A., Foster, K., Hunka, N., Jackson, R. B., Kurz, W. A., Lindquist, A., Liu, M., Luijkx, I., Mialon, A., Michalak, A. M., Miller, J., Obermeier, W. A., Pan, N., Randerson, J. T., Raymond, P. A., Regnier, P., Resplandy, L., Rocher-Ros, G., Rodriguez-Fernandez, N., Rosentreter, J., Salazar-Neira, J. C., Tank, S. E., Tian, H., Vargas, R., Villalobos, Y., Wang, J. A., Wei, X.,

https://doi.org/10.5194/essd-2026-420
Preprint. Discussion started: 21 September 2026


Wickland, K. P., Williams, C., Windham-Myers, L., Woodall, C., Ying, Q., and Zhang, Z.: The North American Greenhouse Gas Budget: Emissions, Removals, and Integration for $CO_2$ , $CH_4$ , and $N_2O$ (2010–2019): Results From the Second REgional Carbon Cycle Assessment and Processes Study (RECCAP2), Glob. Biogeochem. Cycles, 39, e2024GB008310, https://doi.org/10.1029/2024GB008310, 2025.

Qin, X., Tian, H., Canadell, J. G., Shi, Y., Pan, S., Bastos, A., Ciais, P., Crippa, M., Pan, N., Patra, P. K., Poulter, B., Saunois, M., and Sitch, S.: Greenhouse Gas Budgets of Central and West Asia (2000–2020): A Significant Net Source to the Atmosphere, Glob. Biogeochem. Cycles, 39, e2024GB008370, https://doi.org/10.1029/2024GB008370, 2025.

Ren, G., Du, K., Karion, A., Zhao, S., Lopez-Coto, I., Wang, X., Whetstone, J., and Lin, H.: Site selection and effects of background towers on urban CO2 estimates: A case study from central downtown Zhengzhou in China, Environ. Res., 263, 120169, https://doi.org/10.1016/j.envres.2024.120169, 2024.

Saunois, M., Bousquet, P., Poulter, B., Peregon, A., Ciais, P., Canadell, J. G., Dlugokencky, E. J., Etiope, G., Bastviken, D., Houweling, S., Janssens-Maenhout, G., Tubiello, F. N., Castaldi, S., Jackson, R. B., Alexe, M., Arora, V. K., Beerling, D. J., Bergamaschi, P., Blake, D. R., Brailsford, G., Brovkin, V., Bruhwiler, L., Crevoisier, C., Crill, P., Covey, K., Curry, C., Frankenberg, C., Gedney, N., Höglund-Isaksson, L., Ishizawa, M., Ito, A., Joos, F., Kim, H.-S., Kleinen, T., Krummel, P., Lamarque, J.-F., Langenfelds, R., Locatelli, R., Machida, T., Maksyutov, S., McDonald, K. C., Marshall, J., Melton, J. R., Morino, I., Naik, V., O'Doherty, S., Parmentier, F.-J. W., Patra, P. K., Peng, C., Peng, S., Peters, G. P., Pison, I., Prigent, C., Prinn, R., Ramonet, M., Riley, W. J., Saito, M., Santini, M., Schroeder, R., Simpson, I. J., Spahni, R., Steele, P., Takizawa, A., Thornton, B. F., Tian, H., Tohjima, Y., Viovy, N., Voulgarakis, A., Van Weele, M., Van Der Werf, G. R., Weiss, R., Wiedinmyer, C., Wilton, D. J., Wiltshire, A., Worthy, D., Wunch, D., Xu, X., Yoshida, Y., Zhang, B., Zhang, Z., and Zhu, Q.: The global methane budget 2000–2012, Earth Syst. Sci. Data, 8, 697–751, https://doi.org/10.5194/essd-8-697-2016, 2016.

Saunois, M., Stavert, A. R., Poulter, B., Bousquet, P., Canadell, J. G., Jackson, R. B., Raymond, P. A., Dlugokencky, E. J., Houweling, S., Patra, P. K., Ciais, P., Arora, V. K., Bastviken, D., Bergamaschi, P., Blake, D. R., Brailsford, G., Bruhwiler, L., Carlson, K. M., Carrol, M., Castaldi, S., Chandra, N., Crevoisier, C., Crill, P. M., Covey, K., Curry, C. L., Etiope, G., Frankenberg, C., Gedney, N., Hegglin, M. I., Höglund-Isaksson, L., Hugelius, G., Ishizawa, M., Ito, A., Janssens-Maenhout, G., Jensen, K. M., Joos, F., Kleinen, T., Krummel, P. B., Langenfelds, R. L., Laruelle, G. G., Liu, L., Machida, T., Maksyutov, S., McDonald, K. C., McNorton, J., Miller, P. A., Melton, J. R., Morino, I., Müller, J., Murguia-Flores, F., Naik, V., Niwa, Y., Noce, S., O'Doherty, S., Parker, R. J., Peng, C., Peng, S., Peters, G. P., Prigent, C., Prinn, R., Ramonet, M., Regnier, P., Riley, W. J., Rosentreter, J. A., Segers, A., Simpson, I. J., Shi, H., Smith, S. J., Steele, L. P., Thornton, B. F., Tian, H., Tohjima, Y., Tubiello, F. N., Tsuruta, A., Viovy, N., Voulgarakis, A., Weber, T. S., Van Weele, M., Van Der Werf, G. R., Weiss, R. F., Worthy, D., Wunch, D., Yin, Y., Yoshida, Y., Zhang, W., Zhang, Z., Zhao, Y., Zheng, B., Zhu, Q., Zhu, Q., and Zhuang, Q.: The Global Methane Budget 2000–2017, Earth Syst. Sci. Data, 12, 1561–1623, https://doi.org/10.5194/essd-12-1561-2020, 2020.

Saunois, M., Martinez, A., Poulter, B., Zhang, Z., Raymond, P. A., Regnier, P., Canadell, J. G., Jackson, R. B., Patra, P. K., Bousquet, P., Ciais, P., Dlugokencky, E. J., Lan, X., Allen, G. H., Bastviken, D., Beerling, D. J., Belikov, D. A., Blake, D. R., Castaldi, S., Crippa, M., Deemer, B. R., Dennison, F., Etiope, G., Gedney, N., Höglund-Isaksson, L., Holgerson, M. A., Hopcroft, P. O., Hugelius, G., Ito, A., Jain, A. K., Janardanan, R., Johnson, M. S., Kleinen, T., Krummel, P. B., Lauerwald, R., Li, T., Liu, X., McDonald, K. C., Melton, J. R., Mühle, J., Müller, J., Murguia-Flores, F., Niwa, Y., Noce, S., Pan, S., Parker, R. J., Peng, C., Ramonet, M., Riley, W. J., Rocher-Ros, G., Rosentreter, J. A., Sasakawa, M., Segers, A., Smith, S. J., Stanley, E. H., Thanwerdas, J., Tian, H., Tsuruta, A., Tubiello, F. N., Weber, T. S., Van Der Werf, G. R., Worthy, D. E. J., Xi, Y., Yoshida, Y., Zhang, W., Zheng, B., Zhu, Q., Zhu, Q., and Zhuang, Q.: Global Methane Budget 2000–2020, Earth Syst. Sci. Data, 17, 1873–1958, https://doi.org/10.5194/essd-17-1873-2025, 2025.

Schaefer, H.: On the Causes and Consequences of Recent Trends in Atmospheric Methane, Curr. Clim. Change Rep., 5, 259–274, https://doi.org/10.1007/s40641-019-00140-z, 2019.

Schaefer, H., Fletcher, S. E. M., Veidt, C., Lassey, K. R., Brailsford, G. W., Bromley, T. M., Dlugokencky, E. J., Michel, S. E., Miller, J. B., Levin, I., Lowe, D. C., Martin, R. J., Vaughn, B. H., and White, J. W. C.: A 21st-century shift from fossil-fuel to biogenic methane emissions indicated by $^{13}CH_4$, Science, 352, 80–84, https://doi.org/10.1126/science.aad2705, 2016.

https://doi.org/10.5194/essd-2026-420
Preprint. Discussion started: 21 September 2026


Schuldt, K. and et al.: Multi-laboratory compilation of atmospheric methane data for the period 1983-2021; (obspack_ch4_1_GLOBALVIEWplus_v5.1_2023-03-08), https://doi.org/http://doi.org/10.25925/20230308, 2023.

Someya, Y., Yoshida, Y., Ohyama, H., Nomura, S., Kamei, A., Morino, I., Mukai, H., Matsunaga, T., Laughner, J. L., Velazco, V. A., Herkommer, B., Té, Y., Sha, M. K., Kivi, R., Zhou, M., Oh, Y. S., Deutscher, N. M., and Griffith, D. W. T.: Update on the GOSAT TANSO–FTS SWIR Level 2 retrieval algorithm, Atmospheric Meas. Tech., 16, 1477–1501, https://doi.org/10.5194/amt-16-1477-2023, 2023.

Stavert, A. R., Saunois, M., Canadell, J. G., Poulter, B., Jackson, R. B., Regnier, P., Lauerwald, R., Raymond, P. A., Allen, G. H., Patra, P. K., Bergamaschi, P., Bousquet, P., Chandra, N., Ciais, P., Gustafson, A., Ishizawa, M., Ito, A., Kleinen, T., Maksyutov, S., McNorton, J., Melton, J. R., Müller, J., Niwa, Y., Peng, S., Riley, W. J., Segers, A., Tian, H., Tsuruta, A., Yin, Y., Zhang, Z., Zheng, B., and Zhuang, Q.: Regional trends and drivers of the global methane budget, Glob. Change Biol., 28, 182–200, https://doi.org/10.1111/gcb.15901, 2022.

Tanimoto, H., Machida, T., Shirai, T., Niwa, Y., Matsunaga, T., Saeki, T., Yashiro, H., Saigusa, N., Someya, Y., Umezawa, T., Kanaya, Y., Patra, P., Sato, A., Sawa, Y., Suda, K., Kondo, M., Ito, A., Ochiai, O., Suto, H., Okano, S., Ishihara, H., Tsuboi, K., Ohara, K., Takatsuji, S., Kawasaki, T., Kavvada, A., Lefer, B., Boukabara, S. A., Worden, J., Wooldridge, C., Kondragunta, S., Su, W., and Privette, J.: Future Collaboration between the United States and Japan for Possible Development of a Japan GHG Center, Bull. Am. Meteorol. Soc., 106, E197–E203, https://doi.org/10.1175/BAMS-D-24-0275.1, 2025.

Thanwerdas, J., Saunois, M., Berchet, A., Pison, I., and Bousquet, P.: Investigation of the renewed methane growth post-2007 with high-resolution 3-D variational inverse modeling and isotopic constraints, Atmospheric Chem. Phys., 24, 2129–2167, https://doi.org/10.5194/acp-24-2129-2024, 2024.

Thompson, R. L., Stohl, A., Zhou, L. X., Dlugokencky, E., Fukuyama, Y., Tohjima, Y., Kim, S. -Y., Lee, H., Nisbet, E. G., Fisher, R. E., Lowry, D., Weiss, R. F., Prinn, R. G., O'Doherty, S., Young, D., and White, J. W. C.: Methane emissions in East Asia for 2000–2011 estimated using an atmospheric Bayesian inversion, J. Geophys. Res. Atmospheres, 120, 4352–4369, https://doi.org/10.1002/2014JD022394, 2015.

Toha, M., Ariyan, T. N., and Alam, M.: Methane hotspots in landfills: A systematic review on transboundary dispersion and impacts on heatwaves in South Asia, Clean. Waste Syst., 10, 100235, https://doi.org/10.1016/j.clwas.2025.100235, 2025.

Tsuruta, A., Aalto, T., Backman, L., Hakkarainen, J., Van Der Laan-Luijkx, I. T., Krol, M. C., Spahni, R., Houweling, S., Laine, M., Dlugokencky, E., Gomez-Pelaez, A. J., Van Der Schoot, M., Langenfelds, R., Ellul, R., Arduini, J., Apadula, F., Gerbig, C., Feist, D. G., Kivi, R., Yoshida, Y., and Peters, W.: Global methane emission estimates for 2000–2012 from CarbonTracker Europe-$CH_4$ v1.0, Geosci. Model Dev., 10, 1261–1289, https://doi.org/10.5194/gmd-10-1261-2017, 2017.

Turner, A. J. and Jacob, D. J.: Balancing aggregation and smoothing errors in inverse models, Atmospheric Chem. Phys., 15, 7039–7048, https://doi.org/10.5194/acp-15-7039-2015, 2015.

Van Der Laan-Luijkx, I. T., Van Der Velde, I. R., Van Der Veen, E., Tsuruta, A., Stanislawska, K., Babenhauserheide, A., Zhang, H. F., Liu, Y., He, W., Chen, H., Masarie, K. A., Krol, M. C., and Peters, W.: The CarbonTracker Data Assimilation Shell (CTDAS) v1.0: implementation and global carbon balance 2001–2015, Geosci. Model Dev., 10, 2785–2800, https://doi.org/10.5194/gmd-10-2785-2017, 2017.

Wang, F., Maksyutov, S., Tsuruta, A., Janardanan, R., Ito, A., Sasakawa, M., Machida, T., Morino, I., Yoshida, Y., Kaiser, J., Janssens-Maenhout, G., Dlugokencky, E., Mammarella, I., Lavric, J., and Matsunaga, T.: Methane Emission Estimates by the Global High-Resolution Inverse Model Using National Inventories, Remote Sens., 11, 2489, https://doi.org/10.3390/rs11212489, 2019.

Wang, F., Maksyutov, S., Janardanan, R., Ito, A., Morino, I., Yoshida, Y., Someya, Y., Tohjima, Y., Kelly, B. F. J., Kaiser, J. W., Lan, X., Mammarella, I., and Matsunaga, T.: Methane emissions from Australia estimated by inverse analysis using in-situ and Satellite (GOSAT) atmospheric observations, GIScience Remote Sens., 62, 2488595, https://doi.org/10.1080/15481603.2025.2488595, 2025a.

https://doi.org/10.5194/essd-2026-420
Preprint. Discussion started: 21 September 2026


Earth System Science Data
Open Access
Discussions

Wang, X., Gao, Y., Jeong, S., Ito, A., Bastos, A., Poulter, B., Wang, Y., Ciais, P., Tian, H., Yuan, W., Chandra, N., Chevallier, F., Fan, L., Hong, S., Lauerwald, R., Li, W., Lin, Z., Pan, N., Patra, P. K., Peng, S., Ran, L., Sang, Y., Sitch, S., Takashi, M., Thompson, R. L., Wang, C., Wang, K., Wang, T., Xi, Y., Xu, L., Yan, Y., Yun, J., Zhang, Y., Zhang, Y., Zhang, Z., Zheng, B., Zhou, F., Tao, S., Canadell, J. G., and Piao, S.: The Greenhouse Gas Budget of Terrestrial Ecosystems in East Asia Since 2000, Glob. Biogeochem. Cycles, 38, e2023GB007865, https://doi.org/10.1029/2023GB007865, 2024.

Wang, Y., Zhang, Y., Tian, X., Wang, X., Yuan, W., Ding, J., Jiang, F., Jin, Z., Ju, W., Liang, R., Lu, X., Shen, L., Sun, S., Wang, T., Zhang, H., Zhao, M., and Piao, S.: Towards verifying and improving estimations of China's CO2 and CH4 budgets using atmospheric inversions, Natl. Sci. Rev., 12, nwaf090, https://doi.org/10.1093/nsr/nwaf090, 2025b.

Watts, J. D., Ordway, E., Malone, S. L., Zhu, Q., Palmer, P. I., Patel-Tupper, D., Ciais, P., Li, F., Monteverde, D. R., Arndt, K. A., Bruhwiler, L., Buma, B., Cadillo-Quiroz, H., Euskirchen, E., Hoyt, A. M., Holgerson, M., Hugelius, G., Jackson, R. B., Jacob, D., Kuhn, M., Natali, S. M., Peng, S., Perryman, C. R., Poulter, B., Rey-Sánchez, C., Sagang, L. B., Schuur, E. A. G., Varner, R. K., and Vargas, R.: A global methane observation system to track climate feedbacks for verifiable climate impact, Science, 391, 1324–1327, https://doi.org/10.1126/science.aef0459, 2026.

Weber, T., Wiseman, N. A., and Kock, A.: Global ocean methane emissions dominated by shallow coastal waters, Nat. Commun., 10, 4584, https://doi.org/10.1038/s41467-019-12541-7, 2019.

Yadav, V. and Michalak, A. M.: Improving computational efficiency in large linear inverse problems: an example from carbon dioxide flux estimation, Geosci. Model Dev., 6, 583–590, https://doi.org/10.5194/gmd-6-583-2013, 2013.

Yin, Y., Chevallier, F., Ciais, P., Bousquet, P., Saunois, M., Zheng, B., Worden, J., Bloom, A. A., Parker, R. J., Jacob, D. J., Dlugokencky, E. J., and Frankenberg, C.: Accelerating methane growth rate from 2010 to 2017: leading contributions from the tropics and East Asia, Atmospheric Chem. Phys., 21, 12631–12647, https://doi.org/10.5194/acp-21-12631-2021, 2021.

Yoshida, Y., Ota, Y., Eguchi, N., Kikuchi, N., Nobuta, K., Tran, H., Morino, I., and Yokota, T.: Retrieval algorithm for $CO_2$ and $CH_4$ column abundances from short-wavelength infrared spectral observations by the Greenhouse gases observing satellite, Atmospheric Meas. Tech., 4, 717–734, https://doi.org/10.5194/amt-4-717-2011, 2011.

You, H.: China's plan to control methane emissions, Science, 383, 377–377, https://doi.org/10.1126/science.adn4233, 2024.

Yuzhong Zhang and Shuangxi Fang: 2010-2017 China's methane emissions inferred from an inversion of satellite and surface observations2010-2017 China's methane emissions inferred from an inversion of satellite and surface observations (V3), https://doi.org/10.57760/SCIENCEDB.02269, 2022.

Zhang, Y., Fang, S., Chen, J., Lin, Y., Chen, Y., Liang, R., Jiang, K., Parker, R. J., Boesch, H., Steinbacher, M., Sheng, J.-X., Lu, X., Song, S., and Peng, S.: Observed changes in China's methane emissions linked to policy drivers, Proc. Natl. Acad. Sci., 119, e2202742119, https://doi.org/10.1073/pnas.2202742119, 2022.

Zhang, Z., Chen, Z., Zhang, J., Liu, Y., Chen, L., Yang, M., Osman, A. I., Farghali, M., Liu, E., Hassan, D., Ihara, I., Lu, K., Rooney, D. W., and Yap, P.-S.: Municipal solid waste management challenges in developing regions: A comprehensive review and future perspectives for Asia and Africa, Sci. Total Environ., 930, 172794, https://doi.org/10.1016/j.scitotenv.2024.172794, 2024.

Zhao, M., Tian, X., Wang, Y., Wang, X., Ciais, P., Jin, Z., Zhang, H., Wang, T., Ding, J., and Piao, S.: Slowdown in China's methane emission growth, Natl. Sci. Rev., 11, nwae223, https://doi.org/10.1093/nsr/nwae223, 2024.